Phosphate release induced by the reaction of synthetic lepidocrocite (γ-FeOOH) with dissolved sulfide

MSc. thesis - Kevin van Riel (3381269)

22 April 2013

Supervisor:

Dr. Thilo Behrends

Geochemistry
Department of Earth Sciences
Faculty of Geosciences
Utrecht University

Abstract

Reductive dissolution of iron(III) oxyhydroxide minerals is an essential process for regulating the aqueous concentration and mobility of phosphate in natural systems. This is mainly a result of strong specific adsorption of phosphate species onto the particle surface of these minerals, which leads to a release of phosphate to the environment upon dissolution. In order to identify the exact mechanisms of phosphate release during the reductive dissolution reaction of iron(III) oxyhydroxide minerals, multiple flow-through experiments have been performed with synthetic lepidocrocite (γ-FeOOH) and dissolved sulfide. The experimental results are compared to the results from a modeling simulation, which leads to the recognition of two different mechanisms of phosphate release in this case. The process of competitive adsorption can be described as a ligand exchange reaction in which adsorbed phosphate on the lepidocrocite surface is replaced by dissolved sulfide. The kinetics of this process are almost instantaneous for mononuclear complexes, while binuclear complexes of phosphate are replaced much more slowly. Apart from this ligand exchange reaction, phosphate is simply released upon dissolution of iron atoms in its surroundings. This second mechanism accounts for the release of phosphate that is situated in the bulk phase, as well as for adsorbed phosphate release when the kinetics of competitive adsorption are slower than the reductive dissolution rate of lepidocrocite. The influence of pH on the release of phosphate is really prominent, which could be explained based on the speciation of adsorbed phosphate. The relative abundance of mononuclear complexes increases when the pH rises above the isoelectric point, which results in a more instantaneous type of pattern for the release of adsorbed phosphate in higher pH ranges.

Contents

1. Introduction ..... - 4 -
2. Theoretical background ..... - 5 -
2.1. Surface chemistry of iron(III) oxyhydroxides ..... - 5 -
2.2. Adsorption of phosphate ..... - 6 -
2.3. Mechanisms of the reaction between lepidocrocite and dissolved sulfide ..... - 8 -
2.4. Expected mechanisms of phosphate release ..... - 11 -
2.5. Potential retention mechanisms of primarily released phosphate ..... - 12 -
3. Modeling study ..... - 14 -
3.1. Model description ..... - 14 -
3.2. Equilibrium surface speciation of lepidocrocite ..... - 14 -
3.3. Kinetic simulation of the reduction reaction ..... - 17 -
4. Materials and experimental methods ..... - 21 -
4.1. Lepidocrocite and different phosphate pools ..... - 21 -
4.2. Flow-through experiments with sulfide solution ..... - 22 -
4.3. Flow-through experiments with phosphate solution ..... - 23 -
4.4. Analytical techniques ..... - 24 -
5. Experimental results ..... - 26 -
5.1. Adsorption experiments ..... - 26 -
5.2. Breakthrough curves and chemical speciation for the reduction reaction ..... - 27 -
5.3. The release of phosphate ..... - 29 -
5.4. Flow-through experiments with phosphate solution ..... - 31 -
6. Discussion ..... - 32 -
6.1. Bulk phosphate release ..... - 32 -
6.2. The adsorbed phosphate pool ..... - 35 -
6.3. Retention mechanisms of released phosphate ..... - 39 -
7. Conclusions ..... - 40 -
8. References ..... - 41 -
9. Appendix ..... - 43 -

1. Introduction

The reductive dissolution of iron(III) oxyhydroxide minerals is an important process for regulating the concentration of various oxyanions in natural waters. This is mainly due to strong specific adsorption of these ions onto the surface of iron(III) oxyhydroxides, which then results in a release of oxyanions from the particle surface during dissolution of the mineral phase. Iron(III) oxyhydroxide minerals are in general considered as strongly sorbing agents for different oxyanions, such as arsenate, selenite and in particular phosphate (e.g., Hiemstra and Van Riemsdijk, 1999; Chitrakar et al., 2006; Kim et al., 2011; Ding et al., 2012). Due to prominent redox cycling of iron under suboxic conditions, the release of phosphate from iron(III) oxyhydroxides during reductive dissolution is a very important process affecting both the mobility and the cycling of phosphorus through natural environments.

Phosphorus is an essential nutrient for primary producers, but its availability in surface waters is mostly limited. Apart from the adsorption onto iron(III) oxyhydroxides discussed above, phosphate is strongly bound to the surface of aluminium oxyhydroxide minerals and usually coprecipitates with both ferric iron and aluminium oxyhydroxides (e.g., Roncal-Herrero et al., 1996; Tanada et al., 2003). The importance of adsorption and precipitation is typically observed to rise with decreasing pH (e.g., Tanada et al., 2003; Kim et al., 2011). An increased particulate phosphate input from anthropogenic sources often leads to the process of eutrophication (e.g., Chitrakar et al., 2006; Diaz and Rosenberg, 2008; Kim et al., 2011; Ding et al., 2012). This phenomenon is mostly characterized by an increased downward flux of particulate organic matter, which drives enhanced remineralization in the deeper waters (e.g., Diaz and Rosenberg, 2008). This leads to more reducing conditions, which may induce reductive dissolution of iron(III) oxyhydroxide minerals. The accompanying release of particulate phosphate could strongly influence the aqueous phosphorus budget of the concerning system. This process then plays an essential role in enhancing the influence of particulate anthropogenic nutrient inputs on the occurrence of eutrophication in natural waters.

Iron(III) oxyhydroxides are common compounds and are widely spread in natural environments. The most important iron(III) oxyhydroxides in natural systems are goethite (α-FeOOH), lepidocrocite (γ-FeOOH), hematite (α-Fe_2O_3) and the amorphous ferrihydrite phase. Although goethite and hematite are thermodynamically the most stable mineral phases and therefore also show the highest natural abundance, lepidocrocite and the poorly crystalline ferrihydrite usually form upon precipitation from aqueous solution (Cornell and Schwertmann, 1996). The kinetics of the solid phase transformation towards the more stable goethite and hematite phases are often relatively slow, which results in a significant abundance of less stable iron(III) oxyhydroxide minerals. Lepidocrocite was chosen for this study as it is a crystalline phase that is relatively reactive in natural environments, being formed upon oxidation of dissolved ferrous iron (e.g., Canfield, 1989; Cornell and Schwertmann, 1996).

This study aims to investigate the release of phosphate from synthetic lepidocrocite induced by its reaction with dissolved sulfide. The main research question was: “What are the most important mechanisms of phosphate release and what is the influence of pH on these processes?” A theoretical background is provided first, in which the surface chemistry of iron(III) oxyhydroxides is discussed, as well as the mechanisms and the kinetics of the reduction reaction between dissolved sulfide and synthetic lepidocrocite. It is then proposed which mechanisms of phosphate release are the most important during this process, based on the concepts that were introduced. The expected patterns of phosphate release are visualized by the results from a modeling study, in which the reduction reaction was simulated based on the theoretical concepts introduced. These patterns are then compared to the results from various flow-through experiments that were performed at two

different pH values. This consideration should identify the mechanisms of phosphate release during the reaction between synthetic lepidocrocite and dissolved sulfide.

2. Theoretical background

2.1. Surface chemistry of iron(III) oxyhydroxides

In aqueous environments, the surface of iron(III) oxyhydroxide particles is in general characterized by the presence of so-called surface hydroxyl groups. These functional groups are formed as a result of water molecules sharing their lone electron pairs with iron atoms at the particle surface, a process called hydroxylation (e.g., Morel and Hering, 1993; Cornell and Schwertmann, 1996). Depending on the crystal structure and morphology of the solid involved, this process may lead to the formation of singly, doubly and triply coordinated hydroxyl groups (Fig. 2.1). The reactivity of a certain hydroxyl group is then assumed to be influenced by its type of coordination, which is expected to result in the description of iron(III) oxyhydroxide surface chemistry being relatively complicated. However, the difference in reactivity being observed for the differently coordinated hydroxyl groups is relatively large, which rather leads to a relatively simple approach: only the singly coordinated groups are then involved in chemical reactions, while the other groups are simply considered as being unreactive (e.g., Lewis and Farmer, 1986; Kim et al., 2011; Ding et al., 2012).

The singly coordinated surface hydroxyl groups could then be considered as amphoteric species. The corresponding acid-base reactions are generally described as either proton adsorption or desorption (Morel and Hering, 1993): $>FeOH + H^+ = FeOH_2^+$; $>FeOH = >FeO^- + H^+$. The amount of energy related to chemical bonding is in case of these reactions described by an intrinsic acidity constant, which is similar to the acidity constant describing the deprotonation in case of aqueous species. Apart from the amount of energy involved in chemical bonding, the change in free energy for the deprotonation of surface hydroxyl groups also has a contribution from electrostatic interactions, which is due to the presence of an electrical charge on the particle surface (explained below). The so-called apparent ("real") acidity constant then also takes into account the amount of energy that is required for the migration of the protons towards the particle surface in case of the prevailing surface charge. The importance of this electrostatic effect results in the equilibrium thermodynamics of deprotonation reactions being influenced by the presence of specific adsorbates and by the ionic strength. It is therefore not really possible to report single values for the acidity constants in case of the various iron(III) oxyhydroxides.

As already mentioned above, the particle surface of an iron(III) oxyhydroxide is characterized by a certain surface charge. This charge is originated from the various charged surface species that are present at the concerning particle surface, which could be simply (de)protonation related species or other adsorbates. The total surface charge can be calculated by summing up the charge contributions from all these different species. As might be obvious, the total charge of a particle surface generally decreases with increasing pH, which is explained by the desorption of protons. The point of zero charge (PZC) is then simply the pH at which no net surface charge is observed in case of no specific adsorption taking place. The point of zero charge could be calculated from the concerning intrinsic acidity constants, by assuming that the abundance of $>FeOH_2^+$ equals the abundance of $>FeO^-$ in case of pH = PZC. This then results in the following relationship: $PZC = 0.5 (pK_{a1} + pK_{a2})$. When the effect of specific adsorption on surface charge is also taken into consideration, the pH having a net charge of zero is normally referred to as the isoelectric point (IEP).

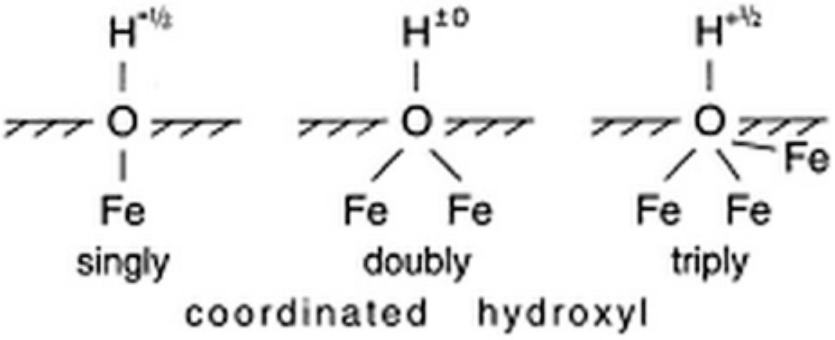

Fig. 2.1. Schematic representation of singly, doubly and triply coordinated surface hydroxyl groups on the surface of an iron(III) oxyhydroxide (Cornell and Schwertmann, 1996).

2.2. Adsorption of phosphate

The adsorption of orthophosphate species onto iron(III) oxyhydroxide surfaces has been studied from two different perspectives, i.e., with a macroscopic and a microscopic approach. Macroscopic studies then mostly focus on the equilibrium distribution (adsorbed or in solution) of orthophosphate being considered as a single species, as well as on the kinetics of the concerning adsorption and desorption processes. The equilibrium distribution of a compound is often visualized as an adsorption isotherm, which shows the adsorbed amount being plotted against the aqueous equilibrium concentration at a certain pH. In case of orthophosphate adsorption onto iron(III) oxyhydroxides, the resulting plots show a relationship that could be described by the so-called Langmuir equation: adsorption increases with increasing aqueous concentration until a certain plateau is reached (Fig. 2.2). This plateau then corresponds to a situation with the particle surface being saturated with orthophosphate. Adsorption edges show the equilibrium distribution of a certain adsorbate depending on the prevailing pH. The adsorption of orthophosphates onto iron(III) oxyhydroxide surfaces is generally observed to increase with decreasing pH, which could be explained by the presence of repulsive forces due to a negative surface charge in higher pH ranges (e.g., Chitrakar et al., 2006; Kim et al., 2011).

Despite the possibility of deriving thermodynamic constants for adsorption from this type of data, applying the resulting description should always remain limited to the specific case of the adsorption experiment. Apart from this, the results from macroscopic studies do not provide any information on the actual mechanism of adsorption or on the speciation of the surface complexes being involved. These two aspects have been investigated in more detail by microscopic studies on orthophosphate adsorption, which use the results from spectroscopic studies in combination with a certain surface complexation model. Three different surface complexes of orthophosphates have been identified on the particle surface of iron(III) oxyhydroxides based on the results from several spectroscopic studies (Tejedor-Tejedor and Anderson, 1990; Kim et al., 2011). The mononuclear monodentate complex is only singly bonded to an iron atom on the particle surface, while two different binuclear bidentate complexes (protonated and deprotonated) are both characterized by the presence of two O-Fe-bonds (Fig. 2.3). The term binuclear then refers to the amount of iron atoms being bound to a single surface complex, while the term bidentate refers to the type of bonding being involved.

The relative abundance of these three different complexes described above is expected to change depending on the prevailing pH (Fig. 2.3). The bidentate complexes ($>Fe_2O_2POOH$ and $>Fe_2O_2PO_2^-$) are the most abundant in the lower and circumneutral pH ranges, but the relative importance of the monodentate complex ($>FeOPO_3^{2-}$) typically increases with increasing pH. This could be explained by a consideration on the surface charge of the iron(III) oxyhydroxide, which leads to a prediction of the

bidentate complexes and the monodentate complex being dominant for respectively a pH below and above IEP (Hiemstra and Van Riemsdijk, 1999). The model presented by these authors was initially developed for goethite, but has also been applied for describing the adsorption of phosphate onto various iron(III) oxyhydroxides in natural environments (e.g., Hiemstra et al., 2010; Weng et al., 2011). The positive surface charge below the IEP favors the type of complexation that introduces a negative charge being situated relatively close to the particle surface. This is then the binding of bidentate complexes, since the presence of two bridging oxygen atoms creates a more negative charge close to the surface when compared to the binding of a monodentate complex (Fig. 2.3). A negatively charged particle surface (for pH>IEP) then results in the monodentate complex being most abundant, since a much less negative charge is introduced closely to the surface upon binding of this complex. The protonation of the bidentate complex could be described by a single acid-base reaction, for which the apparent acidity constant depends on the total surface coverage of phosphate. The negative charge being introduced by the phosphate adsorption results in a stronger affinity for protons as well, which explains the pK-value of the concerning acid-base reaction to rise with increasing surface coverage of phosphate (Hiemstra and Van Riemsdijk, 1996; Hiemstra and Van Riemsdijk, 1999).

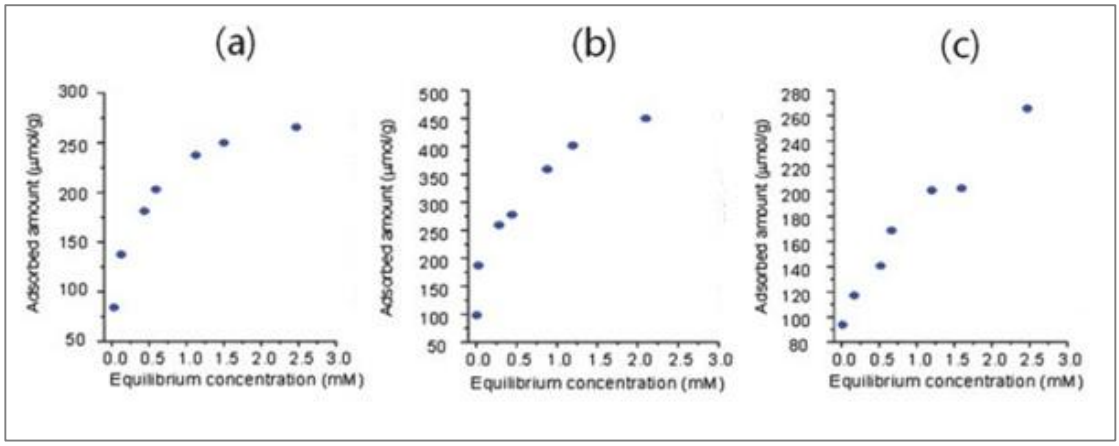

Fig.2.2. Adsorption isotherms for the adsorption of orthophosphates onto the surface of different iron(III) oxyhydroxides - goethite (a), akaganéite (b) and lepidocrocite (c) – at a pH of 5 (Kim et al., 2011).

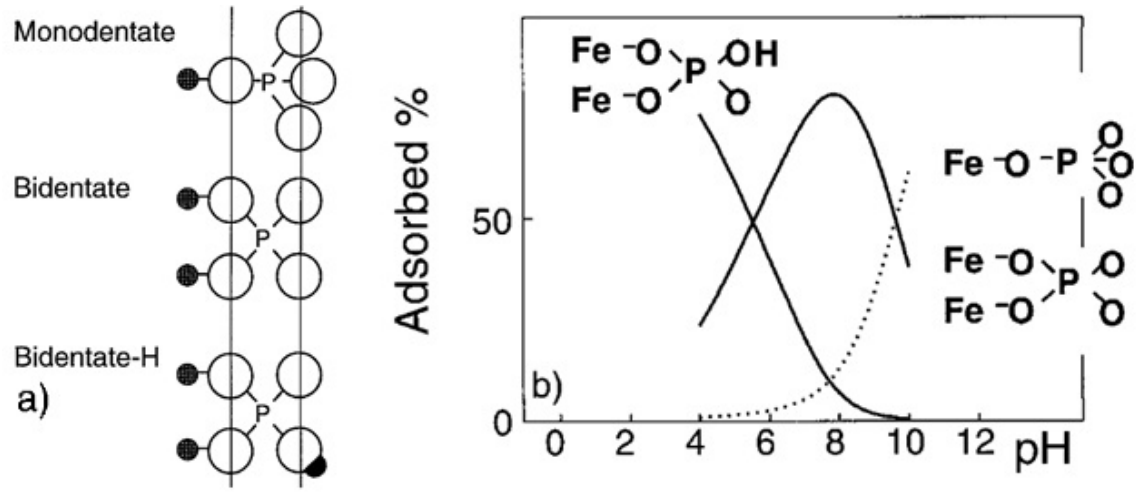

Fig. 2.3. a). Schematic representation of the three different phosphate complexes that have been observed on the surface of iron(III) oxyhydroxides. The open and solid circles respectively represent O- and Fe-atoms, while H-atoms are represented by half a circle in this case. b) Plot showing the relative abundance of these complexes depending on pH, as it was calculated for goethite in a 100 µM phosphate solution with 0.1 M $NaNO_3$ (Hiemstra and Van Riemsdijk, 1999).

Apart from the prevailing pH, the relative abundance of the different orthophosphate complexes on the iron(III) oxyhydroxide surface is also influenced by the total surface coverage of phosphate. The results from spectroscopic and modeling studies both indicate that the relative importance of the monodentate surface complex becomes less with increasing total surface coverage (Tejedor-Tejedor and Anderson, 1990; Hiemstra and Van Riemsdijk, 1999). This could be explained by the introduction of a monodentate surface complex resulting in the development of an anomalously negative charge in the outer electrostatic plane due to the presence of three oxygen atoms (Fig. 2.3). This asymmetric charge distribution may lead to an unstable configuration at a certain point, which is then stabilized by the formation of bidentate surface complexes (Hiemstra and Van Riemsdijk, 1996). However, the observed variation in the speciation of phosphate surface complexes is much larger in case of varying pH.

2.3. Mechanisms of the reaction between lepidocrocite and dissolved sulfide

The reductive dissolution of synthetic lepidocrocite due to its reaction with aqueous sulfide has been experimentally investigated in a number of different studies, focusing on the prevailing mechanisms, the dissolution kinetics and the corresponding reaction products (e.g., Peiffer et al., 1992; Poulton et al., 2004; Hellige et al., 2012). The reaction mechanisms of this process are best visualized by using a reaction scheme, which shows that the concerning process is assumed to take place via a reaction sequence consisting of three consecutive steps (Fig. 2.4). This reaction scheme was first proposed for the reductive dissolution of hematite by dissolved sulfide, but it was shown to be applicable in case of using various iron(III) oxyhydroxides, including lepidocrocite (Dos Santos Afonso and Stumm, 1992; Peiffer et al., 1992). The initial step in the suggested reaction sequence is the formation of sulfide surface complexes by the adsorption of bisulfide ions, which is then followed by reversible electron transfer from sulfur to iron. The $S^{\bullet-}$ radical is released from the surface in the next step, after which it is rapidly further oxidized to higher oxidation state sulfur species (discussed later in more detail). The final reaction step is then the detachment of ferrous iron from the surface, which also creates a new surface site for the adsorption of dissolved sulfide.

$$\equiv FeOH + HS^- \underset{k_{-1}}{\overset{k_1}{\rightleftarrows}} \equiv FeS^- + H_2O \qquad (1)$$

$$\equiv FeS^- \underset{k_{-et}}{\overset{k_{et}}{\rightleftarrows}} \equiv Fe^{II}S^{\bullet}$$

$$\equiv Fe^{II}S^{\bullet} + H_2O \underset{k_{-2}}{\overset{k_2}{\rightleftarrows}} \equiv Fe^{II}OH_2^+ + S^{\bullet-} \qquad (2)$$

$$\equiv Fe^{II}OH_2^+ \xrightarrow[k_3]{H^+} \text{new surface site} + Fe^{2+}_{aq} \qquad (3)$$

Fig. 2.4. Reaction scheme describing the mechanisms of the reaction between aqueous sulfide and iron(III) oxyhydroxides (Dos Santos Afonso and Stumm, 1992).

The first two steps of this reaction scheme are assumed to take place quite instantaneously, while the detachment of ferrous iron from the iron(III) oxyhydroxide surface is generally considered to be the rate limiting step. The concept of ferrous iron release as a final rate limiting step is supported by the results from several experimental studies, which show a significant pool of surface bound ferrous iron being formed (e.g., Poulton, 2003; Poulton et al., 2004; Hellige et al., 2012). Assuming a steady-state concentration for both intermediate species >FeS and $>FeOH_2^+$, the following expression could be derived for the detachment rate of ferrous iron: $v = k_2k_3k_{et}[>FeS^-]/(k_2k_3 + k_{-et}(k_{-2}[S^{\bullet-}] + k_3))$. Since the $S^{\bullet-}$ radical could also be assumed to have a steady-state concentration (because of a fast further oxidation process), this analysis results the overall reaction rate being linearly dependent on the abundance of the sulfide surface complex. The complexation model used for describing this reaction also assumes the existence of protonated sulfide complexes on the iron(III) oxyhydroxide surface (>FeSH), which implies a reductive dissolution process taking place in two parallel reaction pathways (Dos Santos Afonso and Stumm, 1992). The overall reduction rate is then described by the following equation: $v = k_1[>FeS^-] + k_2[>FeSH]$. The parameters k_1 and k_2 in this expression are just constants describing the combined effect of various elementary rate constants and do not directly refer to the rate constants k_1 and k_2 shown in the reaction scheme (Fig. 2.4).

The overall reaction rate of this reductive dissolution process is observed to strongly depend on the prevailing pH, with a maximum value in case of intermediate pH ranges (e.g., Peiffer et al., 1992; Yao and Millero, 1996; Poulton, 2003). In case of lepidocrocite, the appearance of this optimum could be completely explained from its surface speciation and the overall rate equation stated above, when assuming that k_2 is much larger than k_1 (Fig. 2.5). The $>FeS^-$ complex is then only of minor importance for the reductive dissolution process, when compared to the protonated sulfide complex (Peiffer et al., 1992). A more detailed investigation of this relationship - taking into account the presence of other surface species as well - also resulted in these two sulfide complexes being recognized as the most important surface species for the reduction reaction (Yao and Millero, 1996). The potential influence of the aqueous sulfide speciation should also be considered, as is the case for the effect of protonation of the free iron(III) oxyhydroxide surface. Surface protonation may in this case result in a higher reaction rate, which is due to its polarizing effect causing a weakening of the concerning O-Fe-bond (Poulton, 2003).

The overall rate of this reductive dissolution process is generally observed to be linearly dependent on the surface area of the iron(III) oxyhydroxide being involved (e.g., Peiffer et al., 1992; Yao and Millero, 1996; Poulton, 2003). This linear correlation indicates that the reaction is surface controlled, which is in accordance to the proposed reaction scheme (Fig. 2.4). The final expression for the overall reduction rate stated above also supports this observed linearity, with the abundance of the surface complexes being controlled by the total surface area of the iron(III) oxyhydroxide. Apart from surface area, mineralogy has also been identified as an important factor determining the overall reductive dissolution rate. The iron(III) oxyhydroxide minerals with a lower degree of crystal order (including lepidocrocite) are reactive on a time scale of several hours, while the more ordered minerals - such as goethite and hematite - are characterized by a much lower reactivity (Poulton et al., 2004).

As was already mentioned before, the released $S^{\bullet-}$ radical is rapidly further oxidized by other reactive surface sites to higher oxidation state sulfur species. The final speciation of this so-called oxidized product determines the stoichiometry of the overall reduction reaction, which is due to the balance of electrons that has to hold (Table 2.1). The ratio between the amount of sulfide being consumed and the amount of ferric iron reduced is only 0.125 in case of reaching the highest oxidation state (sulfate), while oxidation to elemental sulfur results in a stoichiometric factor of 0.5. Sulfate has been

only sporadically observed during this type of reductive dissolution reaction, which was then in case of a circumneutral or lower pH (Dos Santos Afonso and Stumm, 1992). The results from most other experimental studies rather indicate that elemental sulfur is the dominant oxidized reaction product for all pH ranges (e.g., Peiffer et al., 1992; Yao and Millero, 1996; Hellige et al., 2012).

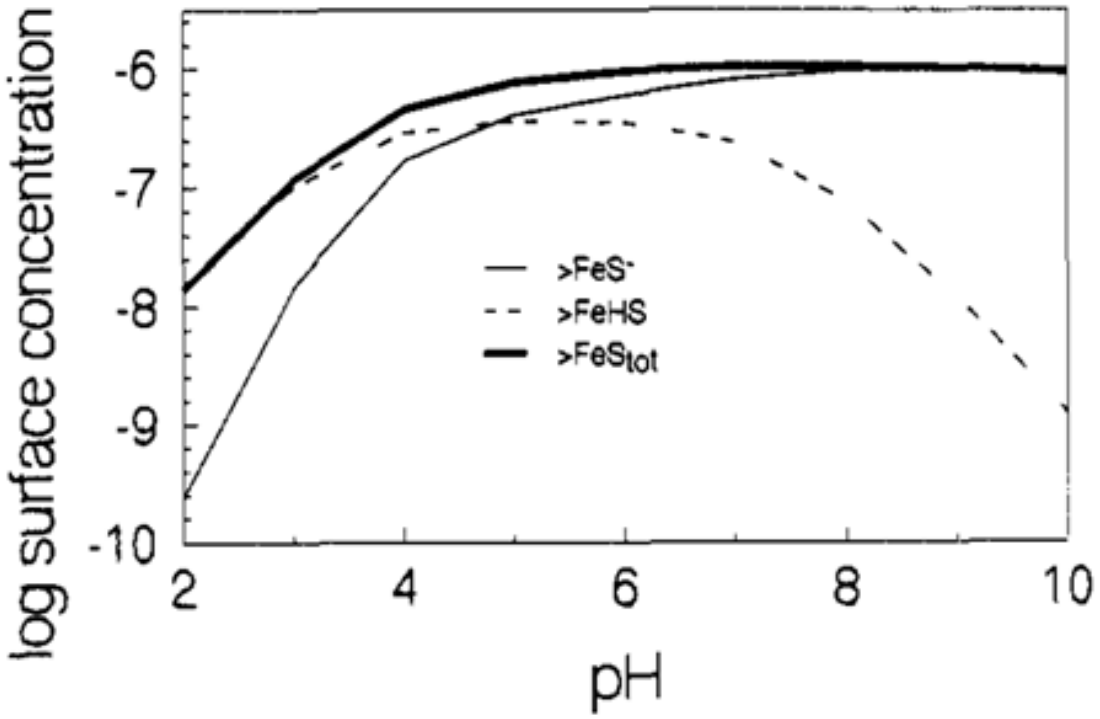

Fig. 2.5. Plot showing the abundance of the different sulfide surface complexes depending on pH (Peiffer et al., 1992).

Table 2.1. List of different final oxidized reaction products with their corresponding stoichiometric factor.

Final oxidized reaction product		ΔFe(III)/ΔS(-II)
Sulfate	SO_4^{2-}	0.125
Sulfite	SO_3^{2-}	0.167
Thiosulfate	$S_2O_3^{2-}$	0.25
Elemental sulfur	S^0	0.5

The fate of the ferrous iron being released from the particle surface is determined by the solubility of iron sulfide minerals. The solid phase being precipitated from an aqueous solution containing both ferrous iron and sulfide is identified as mackinawite (e.g., Rickard and Luther, 2007). In the presence of a significant concentration of aqueous sulfide, the speciation of dissolved ferrous iron is observed to be dominated by the FeS^0 complex in circumneutral and alkaline pH ranges (e.g., Davison et al., 1999; Rickard, 2006). The precipitation of mackinawite could therefore simply be described by the following reaction in this case: FeS^0 = FeS. The precipitation reaction dominating in more acidic environments then involves the free dissolved ferrous iron species, as follows: $Fe^{2+} + H_2S = FeS + 2\ H^+$ (Rickard, 2006). Describing the process of mackinawite precipitation by the combination of these two equilibrium reactions then results in the solubility of mackinawite being independent on pH in case of circumneutral and alkaline environments (Fig. 2.6). This plot shows an equilibrium total aqueous ferrous iron concentration of about 1 µM for a pH of 6 or higher in case of a 1 mM dissolved sulfide concentration. The concentration of the free ferrous iron species is even several orders of magnitude smaller, which is due to the dissolved ferrous iron speciation being dominated by FeS^0 complexes.

The kinetics of mackinawite precipitation from aqueous solution are considered to be very fast, the corresponding reaction could be assumed to take place quite instantaneously (Rickard, 1995). This then results in almost all ferrous iron released being immediately converted into mackinawite. The particle surface of mackinawite is observed to be non-hydrated, with an acid-base chemistry that could be described in terms of the different surface species $>FeSH_2^+$, >FeSH and $>FeS^-$ (Wolthers et al., 2005).

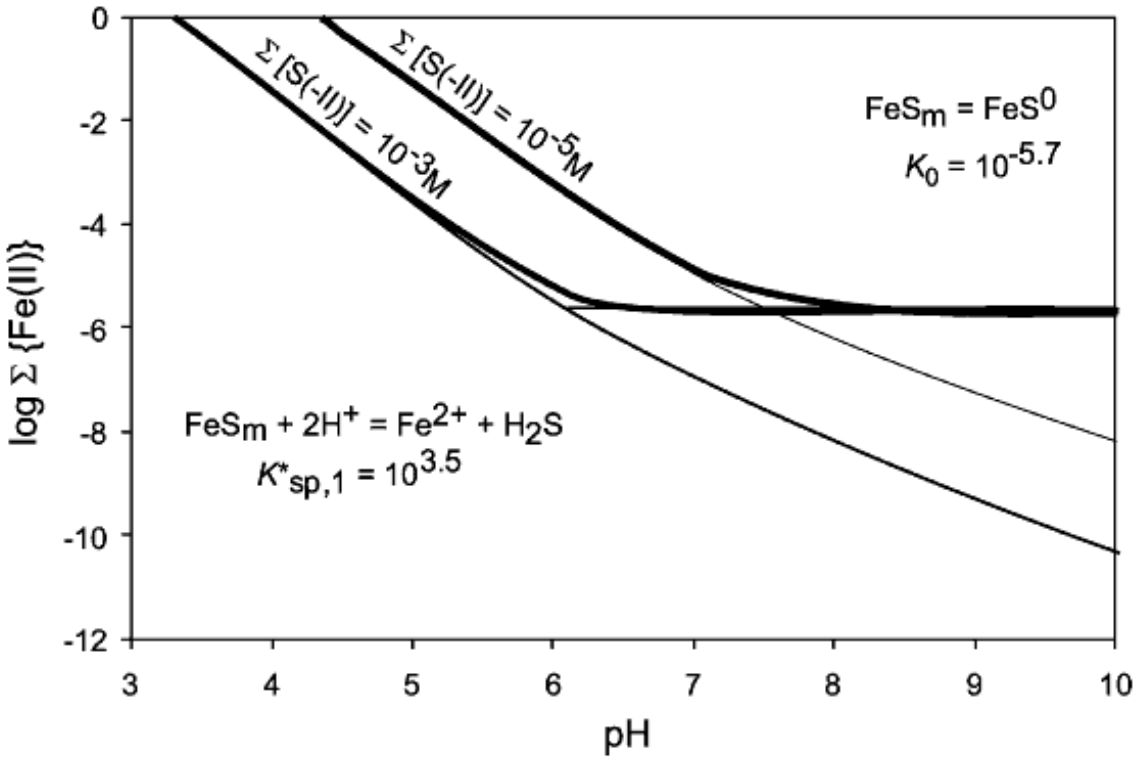

Fig. 2.6. Plot showing both the total level of dissolved ferrous iron (thick lines) and the concentration of the free ferrous iron species (thinner lines) being in equilibrium with mackinawite, for two different aqueous sulfide concentrations (Rickard, 2006).

2.4. Expected mechanisms of phosphate release

Considering the release of phosphate from iron(III) oxyhydroxides during the reaction with dissolved sulfide, two different pools should be distinguished: phosphate bound to the particle surface (section 2.2) and the so-called bulk phosphate. This second type of phosphate is then situated within the bulk phase of the iron(III) oxyhydroxide, as a minor constituent. In this case, release into solution would simply require the phosphate to encounter the solid-water interface. Assuming that the phosphate is evenly distributed over the mineral phase, this results in the rate of bulk phosphate release being linearly dependent on the dissolution rate of the mineral phase itself. The total amount of bulk phosphate released should then also be linearly proportional to the final reaction progress of the reductive dissolution reaction.

The adsorbed phosphate pool is expected to be released due to competitive adsorption of dissolved sulfide species, during the first step of the reductive dissolution process (Fig. 2.4). With bisulfide ions as the most important sulfide species, this competitive adsorption process could be described with a combination of two ligand exchange reactions, for respectively the bidentate and the monodentate surface phosphate complexes: $>Fe_2O_2PO_2^- + 2\ HS^- = 2\ >FeS^- + HPO_4^{2-} + H^+$; $>FeOPO_3^{2-} + HS^- = >FeS^- + HPO_4^{2-}$. The recognition of these two parallel reaction pathways implies a rate of adsorbed phosphate

release that could be described by the equation: $v = k_1[>Fe_2O_2PO_2^-][HS^-]^2 + k_2[>FeOPO_3^{2-}][HS^-]$. The first term in this rate law then refers to the release of phosphate from bidentate surface complexes, while the release from the monodentate complexes is described by the second term. However, it is still not clear whether the ligand exchange should be considered as an elementary reaction in case of a bidentate surface complex being involved. As an alternative approach, competitive adsorption of dissolved sulfide only leads to the formation of a monodentate out of a bidentate surface complex in this case: $>Fe_2O_2PO_2^- + HS^- = >FeOPO_3^{2-} + >FeS^- + H^+$. This would result in an overall rate law without a quadratic dependence on the concentration of bisulfide, but still with two different rate constants: $v = (k_1[>Fe_2O_2PO_2^-] + k_2[>FeOPO_3^{2-}])[HS^-]$. Although the exact mechanism of ligand exchange is unclear in case of a bidentate complex, it is still obvious from this consideration that the release of adsorbed phosphate should be described differently for the monodentate and the bidentate complexes.

2.5. Potential retention mechanisms of primarily released phosphate

After being released into solution, the orthophosphate species might be scavenged by different types of retention mechanisms. Two different processes are considered to be potentially important in case of the reaction between dissolved sulfide and synthetic lepidocrocite: the formation of vivianite and phosphate adsorption onto the surface of mackinawite. As already discussed, the particle surface of mackinawite is non-hydrated and could be described in terms of the abundance of various sulfide surface complexes (Wolthers et al., 2005). Although there are no direct indications for the existence of phosphate complexes on the surface of mackinawite, adsorption of various oxyanion species onto the mackinawite surface has been observed in case of arsenic and selenium (Gallegos et al., 2007; Han et al., 2011). The potential influence of adsorption onto mackinawite as a retention mechanism for aqueous phosphate should therefore be further investigated.

Although the presence of aqueous sulfide results in the dissolved ferrous iron speciation being dominated by FeS^0, this does not directly rule out the formation of vivianite as a potential retention mechanism of primarily released phosphate. The results from thermodynamic calculations indeed indicate that precipitation of vivianite from aqueous solution should be considered as relatively unimportant when the total dissolved sulfide concentration becomes significant (Fig. 2.7). This plot shows that - in case of a 1 µM level of aqueous sulfide - the stability field of vivianite is only reached for a 20 µM or higher dissolved phosphate concentration. Apart from direct precipitation from the aqueous phase, the formation of vivianite out of precipitated mackinawite might also play a role as a retention mechanism for primarily released phosphate. The corresponding chemical equation is as follows: $3\ FeS + 2\ HPO_4^{2-} + H^+ + 8\ H_2O = Fe_3(PO_4)_2 \cdot 8H_2O + 3\ HS^-$, with an equilibrium constant of $10^{1.41}$ (Nriagu, 1971). This process might be particularly important in case of a decreasing level of aqueous sulfide over time. The initial level of dissolved sulfide then favors the precipitation of mackinawite from aqueous solution, but the decrease in concentration rather results in the vivianite phase being favored over mackinawite from a certain point. This would then induce the formation of vivianite out of mackinawite, which also results in an uptake of phosphate from aqueous solution.

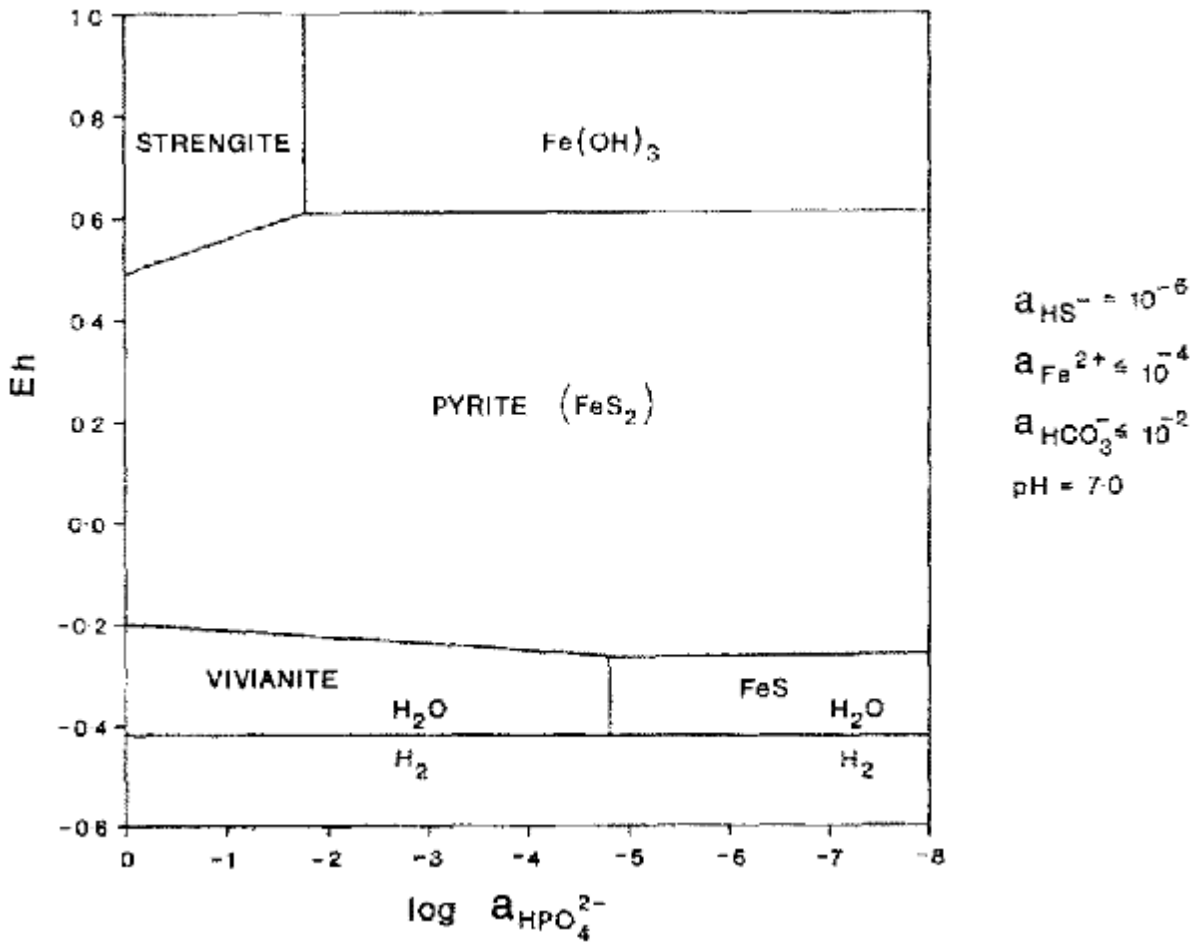

Fig. 2.7. Plot showing the stability fields of the different iron minerals in case of total aqueous sulfide being 1 µM and a dissolved ferrous iron concentration of 10^{-4} M (Nriagu, 1971).

3. Modeling study

3.1. Model description

The different mechanisms of phosphate release stated above were first simulated using the modeling program PHREEQC (Parkhurst and Appelo, 1999). As a first approach, a sulfide solution was introduced to a lepidocrocite surface containing adsorbed phosphate, after which the equilibrium distribution was considered. This should indicate the maximum amount of initially adsorbed phosphate that is expected to be released due to the effect of competitive adsorption. Apart from this equilibrium calculation, a kinetic simulation of the reduction reaction was performed as well, which enabled a consideration on the expected release of bulk phosphate over time. For this consideration, the release of phosphate during the reaction was simply included by using a constant stoichiometric factor. In order to investigate the effect of the pH on these processes of phosphate release, all the modeling simulations were performed for two different pH values (7.5 and 8.5).

The surface complexation calculations performed by the model were all based on the diffuse double layer model, using the thermodynamic constants for hydrous ferric oxide (Dzombak and Morel, 1990) after making some adjustments (Table 3.1). The included protonation and deprotonation constants were changed to values being more characteristic for lepidocrocite (Gupta, 1976). The surface complexation constants for the adsorption of sulfide onto lepidocrocite were added to the hydrous ferric oxide model (Peiffer et al., 1992). The thermodynamic constants for phosphate adsorption were derived from the results from adsorption experiments that were performed with the materials used for the experiments. This was done by fitting the model calculations of phosphate adsorption to the adsorption isotherm that was measured during the first adsorption experiment (for more details see the section on experimental methods). The total concentration of surface sites was calculated from the mass concentration of lepidocrocite and the specific surface area, which was assumed to be 30 m^2/g. The ratio between the abundance of strongly and weakly binding surface sites was assumed to be equal to 1/40 (Dzombak and Morel, 1990).

Table 3.1. The surface complexation reactions included in the model, with the corresponding intrinsic equilibrium constants.

Surface complexation reaction	$\log K_{int}$
$>FeOH + H^+ = >FeOH_2^+$	6.25
$>FeOH = >FeO^- + H^+$	-9.25
$>FeOH + Fe^{2+} = >FeOFe^+ + H^+$ (strongly binding site)	-0.95
$>FeOH + Fe^{2+} = >FeOFe^+ + H^+$ (weakly binding site)	-2.98
$>FeOH + Fe^{2+} + H_2O = >FeOFeOH + 2\ H^+$ (weakly binding site)	-11.55
$>FeOH + PO_4^{3-} + 3\ H^+ = >FeOPO_3H_2 + H_2O$	31.04
$>FeOH + PO_4^{3-} + 2\ H^+ = >FeOPO_3H^- + H_2O$	24.84
$>FeOH + PO_4^{3-} + H^+ = >FeOPO_3^{2-} + H_2O$	18.72
$>FeOH + HS^- = >FeS^- + H_2O$	5.3
$>FeOH + HS^- + H^+ = >FeSH + H_2O$	10.82

3.2. Equilibrium surface speciation of lepidocrocite

In order to identify the maximum amount of adsorbed phosphate being released due to the competitive adsorption of sulfide, the equilibrium surface speciation of lepidocrocite was calculated for two different cases. A free lepidocrocite surface was equilibrated first with a 500 µM phosphate solution containing 0.1 M NaCl as a background electrolyte, at a pH of 8. The mass concentration of lepidocrocite was 10 g/L, such that the conditions were similar to the adsorption experiments

performed (see the section on experimental methods). The resulting equilibrium speciation shows a total surface coverage of about 16% for phosphate, while >FeOH is calculated to be the most abundant surface species (Fig. 3.1).

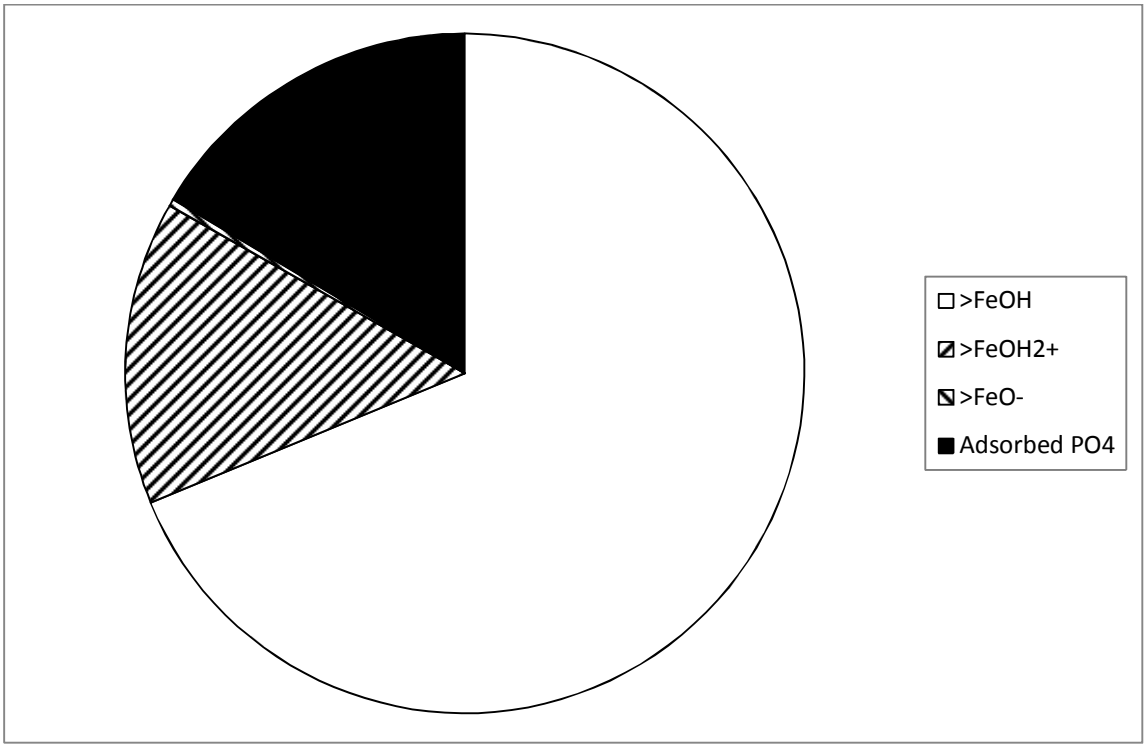

Fig. 3.1. The calculated surface speciation after equilibration with 500 µM phosphate, using 10 g/L of lepidocrocite at pH 8.

The surface speciation calculated in this way was saved, after which a suspension containing 1.25 g/L of the material was equilibrated with a 2 mM total sulfide solution (containing 0.1 M NaCl as a background electrolyte) at both a pH of 7.5 and a pH of 8.5. The relative abundance of lepidocrocite and dissolved sulfide was chosen in such a way that the conditions were similar to the performed flow-through experiments (for more detail, see the section on experimental methods). The corresponding equilibrium surface speciation shows the initially adsorbed phosphate being almost completely substituted by adsorbed sulfide for both pH values (Fig. 3.2). Although the calculated total surface coverage of sulfide is larger for a pH of 7.5 than in case of pH 8.5 (70 % versus 58 %), the effect of the pH on the surface coverage of >FeSH is even much larger (being 20 % versus 4 % for a pH of 7.5 and 8.5 respectively). This already indicates that the reduction reaction should proceed faster for a pH of 7.5, which is in accordance to experimental observations (e.g., Peiffer et al., 1992; Yao and Millero, 1996; Poulton, 2003).

The maximum amount of adsorbed phosphate being released was calculated by comparing both equilibrium surface speciations. The equilibrium distribution with 2 mM total sulfide shows that the adsorbed phosphate is almost completely removed in case of both pH ranges: about 3.1 % of the initial pool remains adsorbed for a pH of 7.5, while this fraction is only 0.9 % for a pH of 8.5. These results indicate that the release of adsorbed phosphate due to competitive adsorption is not limited by equilibrium thermodynamics with 2 mM of total dissolved sulfide. It only depends on the kinetics of the competitive adsorption process whether the complete release of the initially adsorbed pool takes place within the time scale of the reductive dissolution reaction between dissolved sulfide and lepidocrocite.

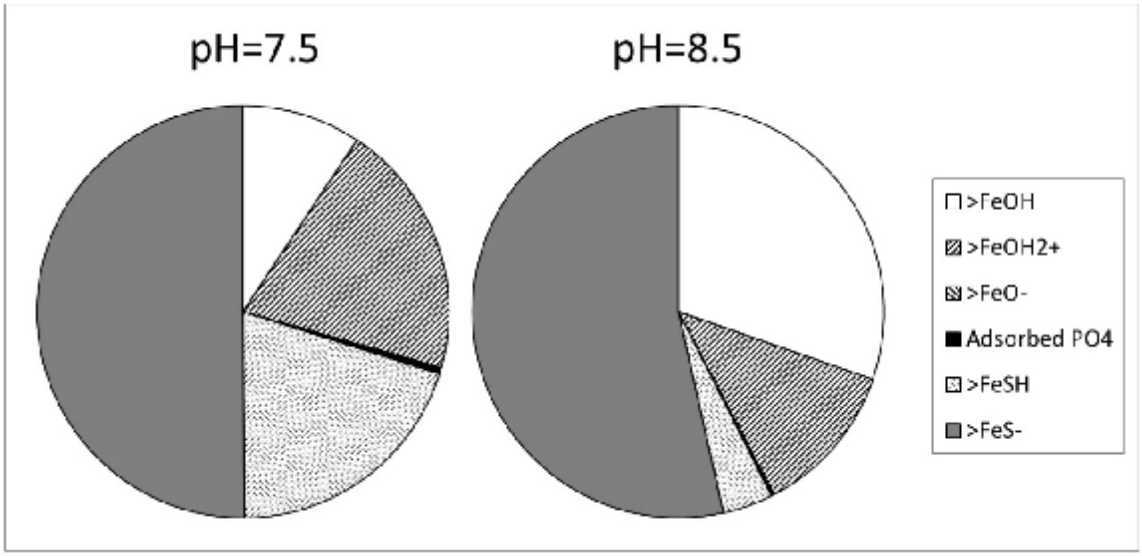

Fig. 3.2. The calculated speciation after equilibrating the surface with 2 mM sulfide at pH 7.5 (left) and pH 8.5 (right).

Although limitation of adsorbed phosphate release due to competitive adsorption by equilibrium thermodynamics is not expected under the experimental conditions (2 mM of total dissolved sulfide), this effect might play a significant role in natural environments, which are mostly characterized by a much lower total level of dissolved sulfide. The fraction of initially adsorbed phosphate remaining on the lepidocrocite surface was calculated after the equilibration with solutions containing different levels of sulfide (Fig. 3.3). This figure shows that only about thirty percent of the initially adsorbed phosphate is released due to competitive adsorption in case of a 20 µM total dissolved sulfide concentration at a pH of 7.5, a limitation which is entirely due to the equilibrium surface speciation of lepidocrocite. The kinetics of the reduction reaction itself are then expected to be most important for determining the release of adsorbed phosphate, instead of the competitive adsorption process. This effect is less pronounced for the higher pH scenario, which still has a maximum adsorbed phosphate release of 57 % due to competitive adsorption for 20 µM of sulfide. These thermodynamic limitations for the competitive adsorption process diminish relatively rapidly with increasing sulfide concentration.

In order to visualize the effect of an instantaneous release of adsorbed phosphate on the concerning breakthrough curve in case of the performed flow-through experiments (see section on experimental methods), the flushing of phosphate out of a well-mixed reactor was simulated using a flow-through model. Assuming that the whole adsorbed phosphate pool is released at once, this results in an initial aqueous phosphate concentration of 23.6 µM (with 1.25 g/L of lepidocrocite). The continuous inflow of background solution (0.1 M NaCl) at a rate of 0.7 mL/min and the accompanying removal of the well-mixed solution were mimicked in PHREEQC by using a combination of a production rate and the dilute function, in such a way that ionic strength was unaffected. The resulting breakthrough curve of phosphate is characterized by a concentration decreasing exponentially over time (Fig. 3.4). Although the release of adsorbed phosphate only takes place at the start of the modeling simulation (t = 0 min), the calculated dissolved phosphate concentration is still significant after the total simulation time of 480 minutes. After a period of 100 minutes, about 25 % of the initially introduced phosphate is still in solution. This analysis already provides some insight into the type of pattern that would be expected for the breakthrough curve of phosphate in case of a complete instantaneous release.

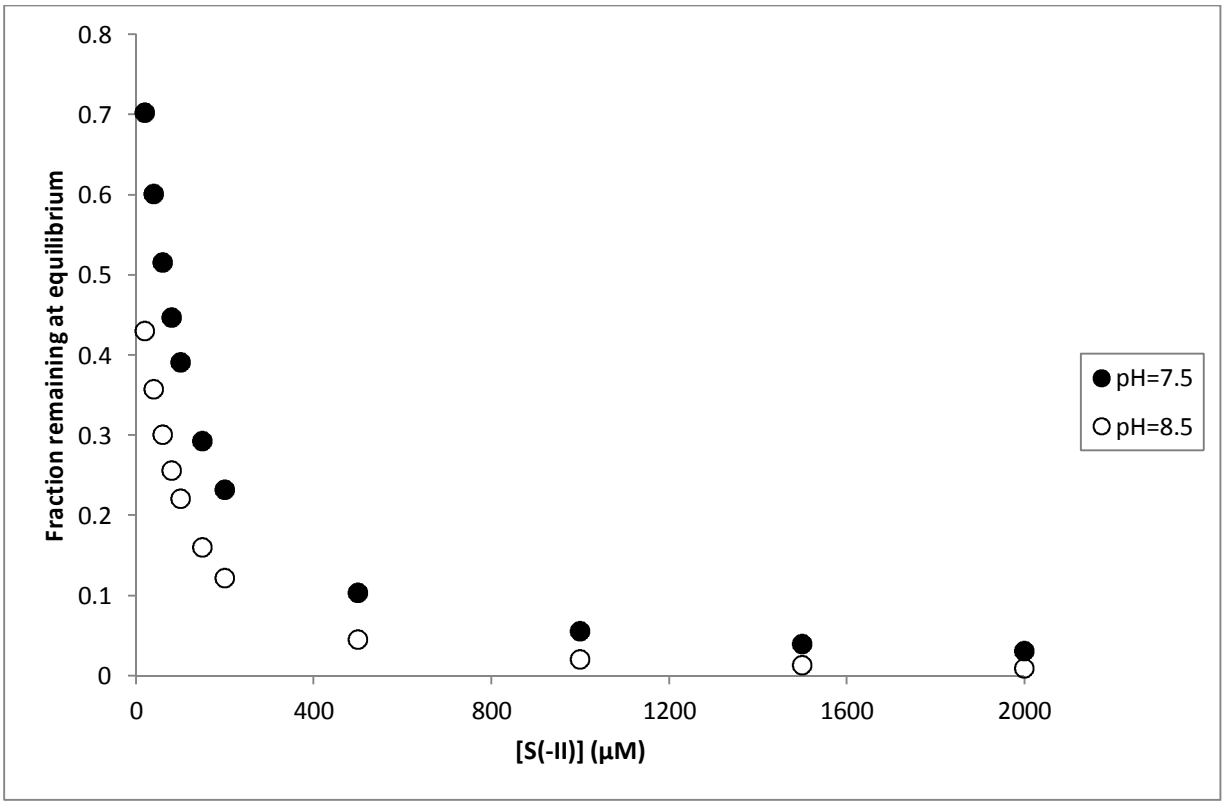

Fig. 3.3. Graph showing the relative amount of initially adsorbed phosphate remained on the lepidocrocite surface at equilibrium, depending on the aqueous concentration of sulfide introduced.

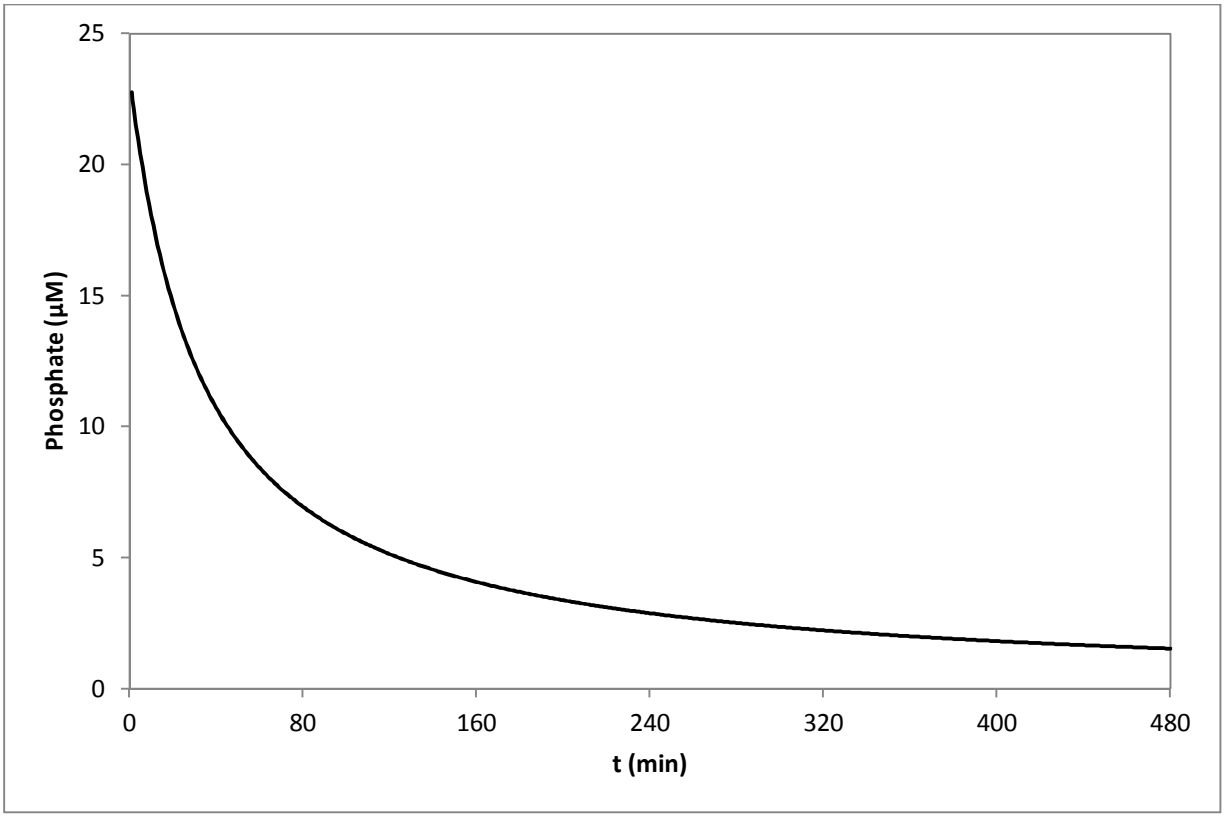

Fig. 3.4. Graph showing the expected pattern for the breakthrough curve of phosphate during the performed flow-through experiments, in case of the adsorbed phosphate pool being instantaneously released at t = 0 min.

3.3. Kinetic simulation of the reduction reaction

Apart from the surface complexation model used for the thermodynamic calculations above, a kinetic model was used for simulating the reduction reaction itself. The release of bulk phosphate as a result of this process was then calculated over time by assuming that the release of phosphate was simply dependent on the reduction rate according to a stoichiometric factor. The reduction rate was calculated from the lepidocrocite surface speciation for each time step, using a rate law that was already described in the theoretical section: $v = k_1[>FeS^-] + k_2[>FeSH]$. The two rate constants were assumed to be 30 h^{-1} and 400 h^{-1} respectively, which was based on the experimental observations for the reduction of hematite by dissolved sulfide (Dos Santos Afonso and Stumm, 1992). Elemental sulfur was assumed to be the only oxidized sulfur species after the reaction, which resulted in the following stoichiometry: $FeOOH(PO_4)_{0.0032} + 2.5\ H^+ + 0.5\ HS^- = Fe^{2+} + 2\ H_2O + 0.5\ S^0 + 0.0032\ PO_4^{3-}$. The included stoichiometric coefficient for phosphate release was based on its relative abundance (compared to iron) in the first type of lepidocrocite used for the experiments (for more detail, see the section on experimental methods).

In order to simulate the breakthrough curves in case of the performed flow-through experiments (see section on experimental methods), the flow into and out of the reactors was simulated in a similar way as done for the consideration on the instantaneous release of the adsorbed phosphate pool. Sulfide was also continuously produced in this case at a constant rate, simulating the inflow of a 2 mM sulfide solution at a flow rate of 0.7 mL/min. The initial lepidocrocite concentration was chosen to be 1.25 g/L and the adsorption of phosphate on its surface was neglected. The pH of the solution was fixed for each time step at a value of either 7.5 or 8.5 (simulating the effect of a buffer solution). Equilibrium with mackinawite was assumed for each time step, since the process of mackinawite formation from aqueous solution is generally considered to be very fast (Rickard, 1995). In order to evaluate the importance of vivianite precipitation as a potential retention mechanism of released phosphate, the saturation index of vivianite was calculated by the model for each time step.

The calculated breakthrough curves clearly show the production of elemental sulfur and phosphate over time (Fig. 3.5). As was expected based on the kinetics of the reduction reaction, the production rates of these species seem to be higher in case of pH 7.5, when compared to a pH of 8.5. The maximum concentration of elemental sulfur is calculated to be about 0.4 mM, while phosphate reaches an almost constant concentration of about 2 µM after 80 minutes. The inflow concentration of sulfide (2 mM) is not reached within the total simulation time of 480 minutes (both for pH 7.5 and pH 8.5), which indicates that the reduction reaction still proceeds at a significant rate at the end of the simulation time. The concentration of dissolved ferrous iron is completely controlled by the equilibrium of the solution with mackinawite, which results in an almost constant value of about 1 µM. This level is in accordance to the expectations based on the solubility of mackinawite, which was discussed in the theoretical section (Fig. 2.6; Rickard, 2006).

The ferrous iron released during the reduction reaction then almost completely precipitates as mackinawite, for which the concentration increases over time up to a value of about 8 mM in case of pH 7.5 (Fig. 3.6). This corresponds to a mass concentration of 0.71 g/L, while the calculated final mass concentration of mackinawite for a pH of 8.5 was about 0.56 g/L. These values indicate that 57 % (pH=7.5) or 44 % (pH=8.5) of the initial lepidocrocite is reduced in a total time period of 480 minutes. The calculated amount of mackinawite formed is similar to the total amount of extractable ferrous iron measured after several hours during the reduction reaction between synthetic lepidocrocite (with similar mass concentration) and a millimolar level of dissolved sulfide (Hellige et al., 2012). This indicates that the rate constants used for this modeling study (which were actually reported for the

reduction of hematite by dissolved sulfide) seem also suitable for describing the reaction between synthetic lepidocrocite and dissolved sulfide.

The calculated saturation indices for the vivianite phase indicate that the formation of vivianite may be considered as being unimportant for the retention of released bulk phosphate (Fig. 3.7). The highest value for the saturation index is about -7, which is calculated in case of pH 7.5. In order to evaluate the potential importance of vivianite formation as a retention mechanism of adsorbed phosphate being released, the maximum aqueous phosphate concentration reached as a result of this release was considered first. This level should be equal to the calculated initial concentration in case of an instantaneous release of the whole pool (23.6 µM; Fig. 3.4), which is about one order of magnitude larger than the calculated concentration due to the release of bulk phosphate. Based on the stoichiometry of the vivianite precipitation reaction, this difference in concentration would only lead to a rise in the saturation index by about two units.

This implies that the importance of vivianite precipitation from aqueous solution should be negligible with an inflow dissolved sulfide concentration of 2 mM. This is in accordance to the expectations based on the concepts discussed in the theoretical section, with vivianite formation being simply unfavorable in sulfide containing environments (Nriagu, 1971). As was stated earlier, a decrease in the level of dissolved sulfide after mackinawite precipitation could still lead to the formation of vivianite out of mackinawite. This process would then be potentially important as a retention mechanism of released phosphate.

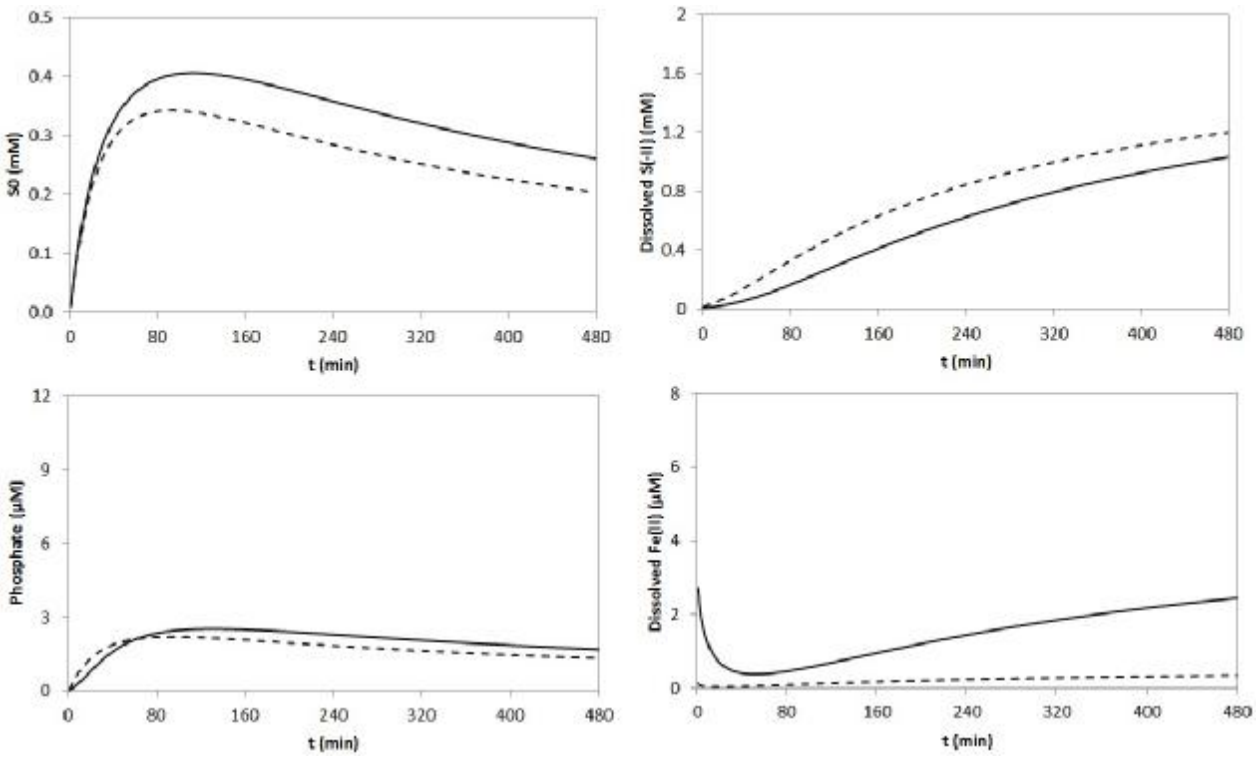

Fig. 3.5. Graphs showing the calculated total concentrations of elemental sulfur, phosphate, dissolved sulfide and dissolved ferrous iron over time. The solid lines show the results for a pH of 7.5, while the dashed lines are for a pH of 8.5.

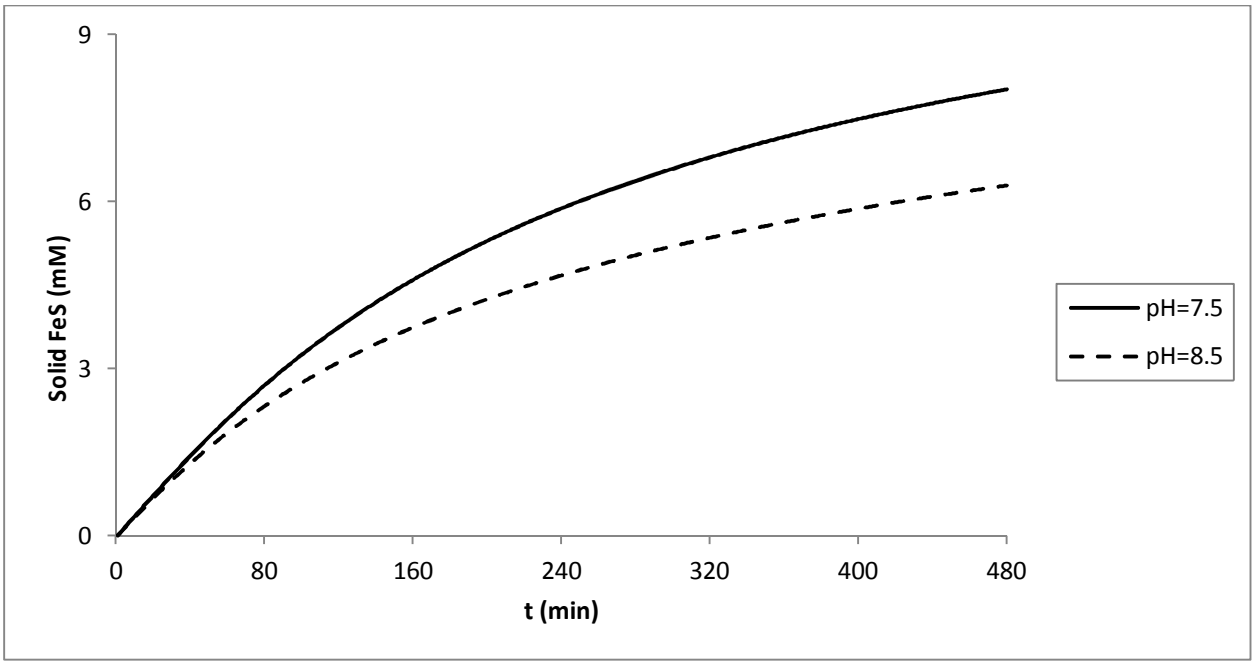

Fig. 3.6. Graph showing the calculated concentration of mackinawite over time, for both a pH of 7.5 and a pH of 8.5.

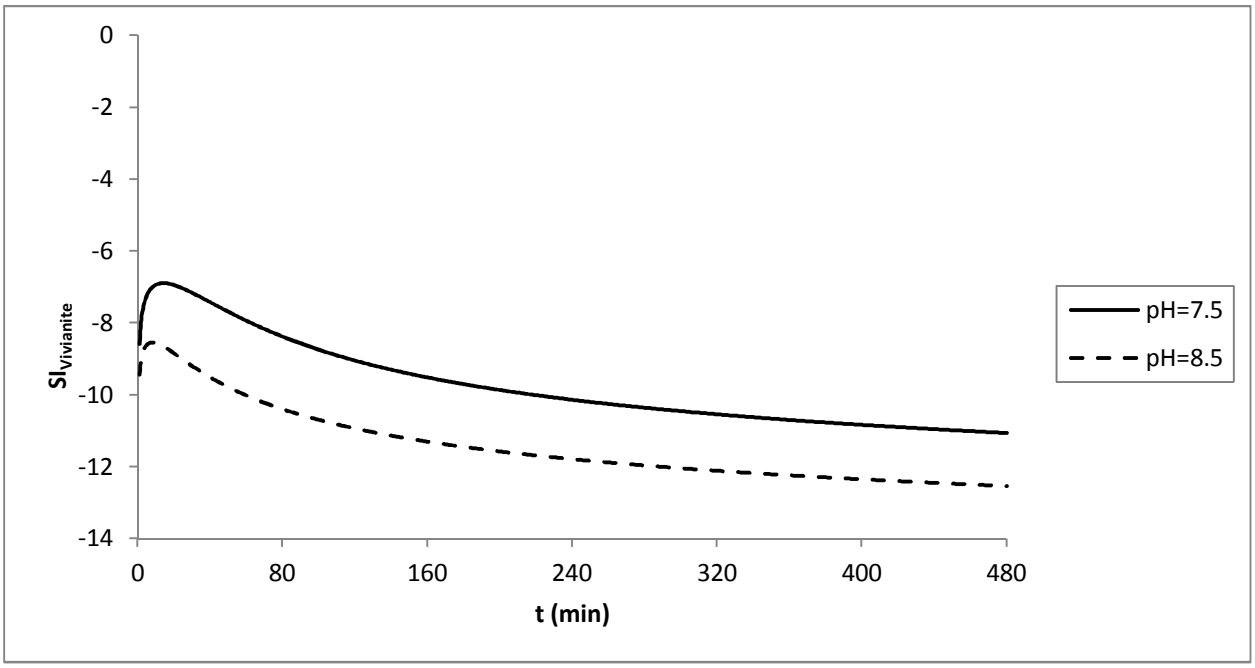

Fig. 3.7. Graph showing the calculated saturation index for vivianite over time in case of [S(-II)] = 2 mM.

4. Materials and experimental methods

4.1. Lepidocrocite and different phosphate pools

Two different types of synthetic lepidocrocite (γ-FeOOH) were used for the experiments described below, which are referred to as type 1 and type 2. The first type of lepidocrocite was purchased from Lanxess (Leverkusen, Germany) and contained a significant amount of phosphorus. Its phosphorus content was determined exactly with Inductively Coupled Plasma-Optical Emission Spectrometry (ICP-OES), which resulted in a molar P/Fe ratio of 3.21 mmol/mol. In order to remove any adsorbed phosphate from its surface, the material was suspended into 0.1 M NaCl, after which the pH was adjusted to a value of 11 by adding NaOH. After a period of 24 hours, the suspension was washed with demi water several times, until the ionic strength was reduced by a factor of about 10^3. The composition of the material was measured afterwards with ICP-OES, which resulted in a similar molar ratio between P and Fe. This indicated that the initially abundant phosphorus pool was similar to the bulk type of phosphate described in the previous sections.

The second type of lepidocrocite used was a suspension that was prepared from a 39.76 g/L $FeCl_2$ solution (Schwertmann and Cornell, 2000). After filtration through a 0.2 µm cellulose acetate membrane filter (in order to remove any akaganéite formed), this solution was purged with argon for 30 minutes at a rate of 200 mL/min. The pH was then adjusted to a value of 6.8 by adding NaOH, which resulted in the formation of a greenish precipitate. The synthesis of lepidocrocite was started by changing the gas stream to air (at a rate of 300 mL/min). Despite using a pH-stat device during the synthesis, the pH was observed to decrease to a constant value of 5.5. The synthesis stopped after about 3 hours, which resulted in a pH increase (to a value of 6.8) and the color of the solid changing from greenish to orange. Both materials (type 1 and type 2) were confirmed to be lepidocrocite by analysis with X-Ray Diffraction (XRD).

Prior to the flow-through experiments described below, a phosphate adsorption experiment was performed for both types of lepidocrocite. In case of the first adsorption experiment, nine suspensions were prepared by adding 2 grams of lepidocrocite (type 1) to 200 mL of a 0.1 M NaCl solution containing 0.02 M of the HEPES buffering agent, after which the pH was adjusted to a value of 8 by adding HCl. Different amounts of a 0.1 M Na_2HPO_4 stock solution were then added to these suspensions, such that the concentration of phosphate ranged from 0 to 500 µM. The suspensions were then shaken continuously at 110 rpm on a horizontal shaker, after which the concentration of phosphate was measured in the solutions that were collected by filtration of the suspensions. With concentrations remaining constant over time (comparing the results measured after 3 days and after 7 days), the lepidocrocite suspensions were assumed to be in equilibrium. The amount of phosphate adsorbed was then calculated from the difference in phosphate concentration for the lepidocrocite suspensions and a set of blank samples, which did not contain any lepidocrocite.

The nine suspensions for the second adsorption experiment were prepared by diluting the original lepidocrocite suspension (type 2) with the NaCl solution described above, such that the lepidocrocite content was 8.5 g/L. The pH was again adjusted to a value of 8 by adding HCl, after which different amounts of the 0.1 M Na_2HPO_4 stock solution were added. The initial concentrations of phosphate used for this experiment again ranged from 0 to 500 µM. The analyses for dissolved phosphate occurred after 7 days and after 11 days in case of this experiment, which provided similar results. The measured concentrations were assumed to represent the equilibrium distribution for the concerning lepidocrocite suspensions.

4.2. Flow-through experiments with sulfide solution

In order to study the kinetics of the reaction of synthetic lepidocrocite with dissolved sulfide and the accompanying release of phosphate, several experiments with flow-through reactors were performed (Table 4.1). This table lists the type of lepidocrocite used and the exact concentration of dissolved sulfide in the inflow solution for each experiment (which was about 2 mM each time), as well as two different pH values that are explained in more detail below. For each experiment, a set of closed flow-through reactors (volume = 24 mL) was filled with lepidocrocite suspension, such that the concentration of lepidocrocite was about 1.25 g/L in case of a full reactor. The suspensions used for these flow-through experiments were taken from the two adsorption experiments described above. For each experiment, half the amount of the reactors was filled with the original lepidocrocite suspension (either type 1 or type 2), while the other reactors were filled with one of the suspensions containing adsorbed phosphate. This set-up enabled a separate study on the potential release of bulk phosphate and adsorbed phosphate (by respectively considering lepidocrocite type 1 after and lepidocrocite type 2 prior to the adsorption of phosphate). The situations without phosphate and with both types of phosphate present were also included in this way.

The inflow into the reactors occurred at a constant rate by using an Ismatec IPC-N microprocessor controlled dispensing pump, which connected the reactors with a homemade gas tight bag equipped with a three port valve. These type of bags were produced from PP/Al/PE foil, which was purchased from Tesseraux Spezialverpackungen GmbH. The inflow solution was stored in such a bag being isolated from the atmosphere, so that dissolution of atmospheric oxygen into the solution was prevented. In order to remove any initially dissolved phosphate from the system, three reactor volumes of a background solution were pumped through the reactor prior to the reaction with dissolved sulfide. Apart from 0.1 M NaCl as a background electrolyte, this solution contained the HEPES-Na buffering agent with a concentration of 0.02 M. For different experiments, the pH of the solution was adjusted to either a value of 7 or 8 by adding HCl (Table 4.1). The achieved solution was then deoxygenated by bubbling argon through it for at least one hour, after which it was stored in the homemade gas tight bag described above.

The inflow solutions with dissolved sulfide were prepared from the background solution by adding a 0.2 M Na_2S stock solution, which occurred under anoxic conditions in a N_2-purged glovebox. The exact concentration of dissolved sulfide was measured afterwards for each experiment. The pH was also measured again after preparing the inflow solutions, since it might have changed due to adding sulfide stock solution. The achieved solutions were stored in a homemade gas tight bag (described above) until using them for the different flow-through experiments (Table 4.1). For each experiment, the inflow solution with sulfide was pumped through the reactors for about 8 hours at a constant pumping rate of 0.7 mL/min. During this period, the solutions in the reactors were well-mixed as a result of continuous stirring with a magnetic stirrer at a constant rate. Outflow from the reactors occurred through a set of two glass fiber filters and a cellulose acetate membrane filter with a pore size of 0.2 µm.

The background solution pumped through the reactors (prior to the reaction with dissolved sulfide) was collected and analyzed for dissolved phosphate. During the reaction, three different types of samples were taken from the outflow for each reactor. For the first type of sample, the outflow solution was collected for 3 minutes in 3 mL of the diamine reagent (more detailed description is in the section on analytical techniques), which was used as a trap to prevent outgassing of dissolved sulfide. The samples collected in this way were analyzed for the concentration of dissolved sulfide. After taking this type of sample, the outflow solution itself was collected for 4 minutes to measure

the pH with a pH-electrode. Another type of sample was collected for 20 minutes in a polyethylene tube containing 200 µL of 6 M HCl. Argon was then continuously bubbled through the solution, in order to remove dissolved sulfide. This type of sample was used for measuring the concentration of elemental sulfur, dissolved ferrous iron and phosphate. The sampling sequence described above was repeated until the end of the experiments.

After the reaction with dissolved sulfide, the suspensions in the reactors were completely dissolved by pumping concentrated HCl (32 %) through the reactors. The resulting outflow was collected for each reactor, with argon being continuously bubbled through the samples. The samples obtained in this way were analyzed for both extractable ferric and ferrous iron (after 50 times dilution), as well as for total extractable phosphate. The exact volume collected was determined afterwards for all the collected samples described above. This enabled an evaluation of the mole balance for all elements involved, as well as the mole balance for the electrons transferred.

Table 4.1. Summarized description of the different flow-through experiments with sulfide solution that were performed.

Exp. no.	Lepidocrocite type	$pH_{background}$	pH_{inflow}	$[S(-II)]_{inflow}$ (mM)
1	1	8	8.46	1.99
3	1	7	7.33	1.95
4	1	7	7.21	1.92
5	2	7	7.09	2.04
6	1	8	8.31	1.97
7	2	8	8.39	2.22

4.3. Flow-through experiments with phosphate solution

The importance of the different mechanisms proposed for the retention of phosphate (adsorption onto the mackinawite surface and the formation of vivianite) was evaluated by performing flow-through experiments with an inflow solution containing dissolved phosphate. These experiments were performed with some of the reactors from the previously described flow-through experiments with dissolved sulfide (containing a suspension without adsorbed phosphate), after the total reaction time of about 8 hours (Table 4.2). In case of using a reactor for this second flow-through experiment, the complete extraction of the solid from the reactor with concentrated HCl was performed after the second experiment.

The potential of the reactors to take up phosphate from the inflow solution was then compared between the reactors from the first flow-through experiment and some other reactors, containing the original lepidocrocite suspension (prior to the reaction with dissolved sulfide). In order to visualize the effect of phosphate uptake on the concentration of dissolved phosphate in the outflow solution from the reactors, this flow-through experiment was also performed using a reactor that only contained the background solution.

The inflow solutions for these flow-through experiments were prepared by adding 150 µL of the 0.1 M Na_2HPO_4 stock solution to 1.0 L of the background solution described in the previous section, which occurred in a N_2-purged glovebox. This inflow solution was pumped through the reactors at a constant pumping rate of 1.74 mL/min for a total time period of 50 minutes. The outflow solution was sampled every 5 minutes for each reactor, after which the resulting samples were analyzed for dissolved phosphate. After this second flow-through experiment, concentrated HCl (32 %) was pumped through the reactors to completely dissolve the suspensions. The resulting outflow was collected with argon being continuously bubbled through the samples, after which the samples were analyzed for total extractable phosphorus, as well as the total extractable iron species in case of the

reactors that were also used for the first flow-through experiment. Similarly to the flow-through experiment with dissolved sulfide, the volumes of all samples were determined by weighing the samples. This enabled a consideration on the total amount of phosphate taken up by the different reactors.

Table 4.2. Summarized description of the different flow-through experiments with phosphate solution that were performed.

Exp. no.	Lepidocrocite type	pH_{inflow}	$pH_{reaction}$	$[S(-II)]_{reaction}$ (mM)
4	1	7	7.21	1.92
5	2	7	7.09	2.04
6	1	8	8.31	1.97
7	2	8	8.39	2.22

4.4. Analytical techniques

The concentrations of sulfide reported for the inflow solutions of the different flow-through experiments were determined by titration (Table 4.1 and 4.2). About 4 mL of the inflow solution (the exact volume was measured each time) were added to an excess iodine solution, immediately after being extracted from the gas tight bag in which the inflow solution was stored. This iodine solution was prepared in an Erlenmeyer flask by mixing 800 µL of standard 0.1 N KIO_3 solution with about 20 mL of demi water, 500 µL of 9 N H_2SO_4 and an excess of KI. The remaining iodine (after the reaction with sulfide) was then back-titrated with a 0.010 N sodium thiosulfate solution (Lawrence et al., 2000).

The sulfide concentrations in the outflow solutions from the reactors were measured colorimetrically with an adjusted version of the methylene blue method (Lawrence et al., 2000). The diamine reagent used was prepared by dissolving 10 grams of N,N-dimethyl-p-phenylenediamine dihydrochloride and 15 grams of $FeCl_3 \cdot 6H_2O$ into 500 mL 6 M HCl. As mentioned before, this reagent was used as a trap when collecting the samples, in order to prevent outgassing of the dissolved sulfide. Analysis of the collected samples then occurred after diluting them for 21 times. The calibration line used was based on standard samples for which the dissolved sulfide concentration was measured with the titrimetric method described above and was linear up to a concentration of at least 2 mM.

Dissolved ferrous iron in the outflow solutions collected during the flow-through experiments was determined using the revised ferrozine method (Viollier et al, 2000). The reagent used contained 10 mM of dissolved ferrozine and 0.1 M of ammonium acetate. For each measurement, 1.2 mL of the concerning sample was added to 200 µL of this reagent, as well as 300 µL demi water and 200 µL of a buffer solution containing 5 M of dissolved ammonium acetate at a pH of 9.5. The absorbance of the samples was then measured at a wavelength of 562 nm, which provided a linear calibration line up to a ferrous iron concentration of at least 120 µM. The amount of extractable ferrous iron present after the reaction with dissolved sulfide was measured with this method as well. Total extractable iron was also measured for these samples, by adding 300 µL of 2.8 M hydroxylamine hydrochloride solution (containing 2 M HCl) instead of 300 µL demi water. The amount of extractable ferric iron after the reaction was then calculated as the difference between the amount of total iron and ferrous iron observed.

Dissolved phosphate in the samples collected during the flow-through experiments was measured using the ascorbic acid method (Koroleff, 1983). The first type of reagent used was freshly prepared prior to each measuring sequence by mixing 6.75 mL of 95 g/L ammonium heptamolybdate solution with 750 µL of 32.5 g/L $KSbOC_4H_4O_6$ solution and 30 mL of 9 N H_2SO_4. The ascorbic acid reagent was also freshly prepared each time by dissolving 0.7 g ascorbic acid into 10 mL of demi water. 2 mL of

the concerning sample were added to 200 µL of both reagents for each measurement, after which the absorbance was measured at a wavelength of 880 nm. The calibration line used was separately measured for each set of samples and was usually linear up to a dissolved phosphate concentration of at least 100 µM. Total extractable phosphorus at the end of the flow-through experiments was determined with ICP-OES.

The method for measuring elemental sulfur in the outflow solutions from the reactors was based on the specific absorption spectra observed for elemental sulfur in different organic solvents, which are typically characterized by a peak of maximum absorption in the ultraviolet range (Eckert and Steudel, 2003). In case of this method, the peak of maximum absorption for elemental sulfur in toluene was identified first by dissolving sulfur powder into toluene and analyzing the absorption spectrum with a UV/VIS spectrophotometer. The resulting spectrum showed a distinct peak of maximum adsorption, which was situated at a wavelength of 308 nm (Fig. 4.1). The calibration line used (relating the elemental sulfur concentration in toluene to the absorbance measured) was linear up to a concentration of at least 3.5 mM.

Elemental sulfur was extracted from the outflow solutions by adding 5 mL of toluene to each sample and shaking them for 5 minutes. This occurred directly after the samples were collected from the outflow of the reactors. After a period of stabilization of at least 30 minutes, the toluene phase was separated from the aqueous phase and stored in a crimp glass bottle until further analysis. After measuring the elemental sulfur concentration in toluene with the method described above, the elemental sulfur content for the aqueous phase was calculated from this value by using the volume of the original sample.

In case of analyzing the outflow solutions from a reactor for dissolved sulfate and thiosulfate species, these measurements were performed with the same samples as used for measuring iron, phosphate and elemental sulfur. Both sulfate and thiosulfate were then measured by using ion chromatography after ten times dilution.

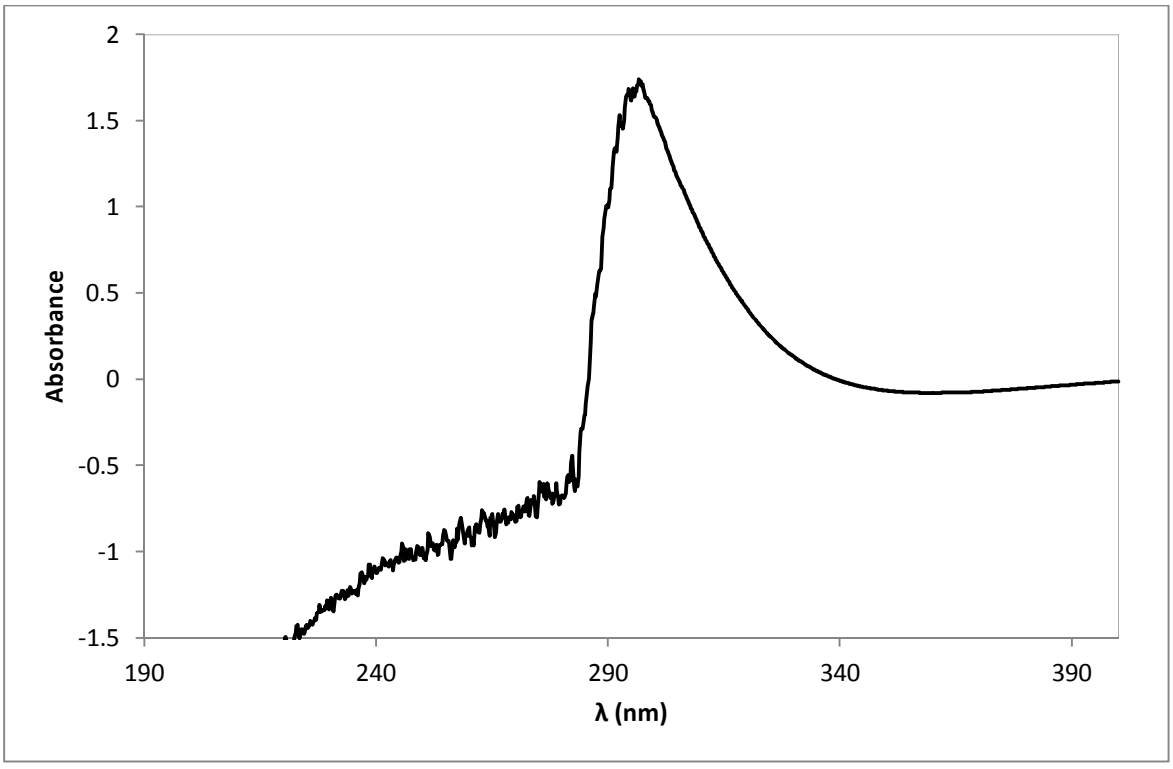

Fig. 4.1. The absorption spectrum that was measured for elemental sulfur being dissolved in toluene.

5. Experimental results

5.1. Adsorption experiments

The results from the phosphate adsorption experiments are included as two different adsorption isotherms, showing the equilibrium surface coverage plotted against the measured equilibrium phosphate concentration (Fig. 5.1). The second type of lepidocrocite is observed to have an about two times larger adsorption capacity, with values for the equilibrium surface coverage up to about 50 µmol/g. The initial amount of phosphate introduced (500 µM) was almost completely taken up in this case, while a maximum equilibrium phosphate concentration of about 250 µM was measured for the first lepidocrocite. The samples used for the flow-through experiments contained 21.5 µmol/g of adsorbed phosphate in case of lepidocrocite type 1 (additional to the bulk phosphate pool), while the surface coverage of phosphate was 53.5 µmol/g in case of using lepidocrocite type 2. This difference should be taken into account when considering the release of adsorbed phosphate during the flow-through experiments.

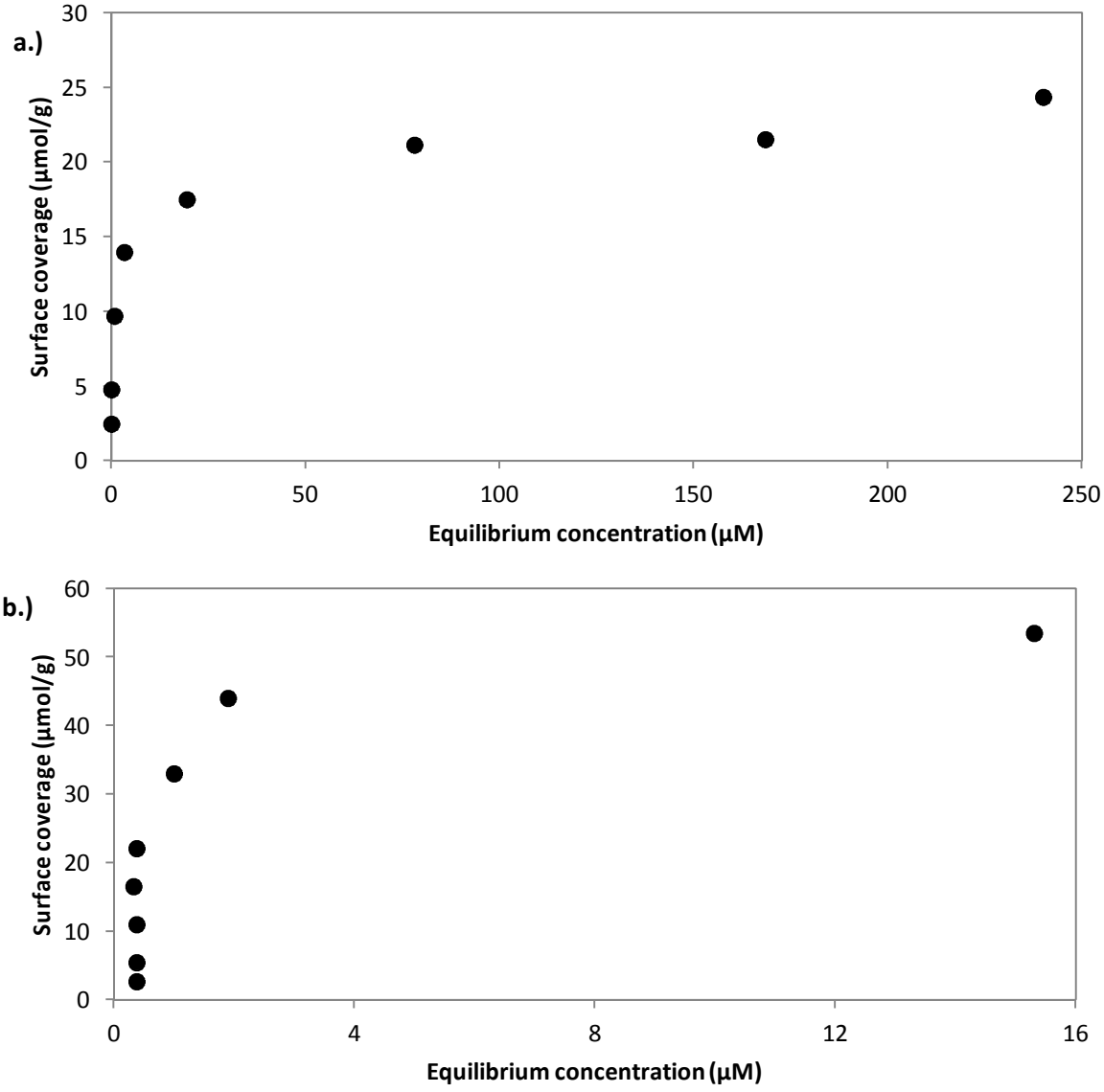

Fig. 5.1. The measured adsorption isotherms for the adsorption of phosphate onto the surface of lepidocrocite type 1 (a.) and lepidocrocite type 2 (b.) at a pH of 8 (I = 0.1 M NaCl).

5.2. Breakthrough curves and chemical speciation for the reduction reaction

The data presented in this section are considered to be representative for all the flow-through experiments performed in the two different pH ranges (Table 4.1). A complete overview of the results is included separately for each experiment in the appendix at the end of this report. Dissolved sulfide was often observed to be removed from solution in the reactors for a significant period of time in case of pH 7.5, while an almost constant concentration of about 1.3 mM was observed for a pH of 8.5 (Fig. 5.2). In case of pH being around 7.5, sulfide was observed to increase again after being removed, reaching a level of about 1.3 mM after the total reaction time of almost 500 minutes. The difference in sulfide concentrations between the two pH ranges implies a faster reduction rate at pH 7.5, similar to the results from the modeling simulation. The elemental sulfur content measured for the outflow solutions was quite constant over time, showing a concentration of about 0.1 mM.

Two completely different patterns were observed for the level of ferrous iron in the outflow solutions over time. The first pattern is represented by reactor 7.4 (Fig. 5.2) and shows ferrous iron concentrations being constant at a micromolar level, which could be expected based on the solubility of mackinawite (Fig. 2.6; Rickard, 2006). The color of the suspension in the reactors was generally observed to change from orange to black during the reaction, which indicates that the ferrous iron produced was indeed mostly retained as mackinawite. The second pattern observed for ferrous iron in the outflow solutions (represented by reactor 5.6 in fig. 5.2) is characterized by the presence of a concentration pulse showing a much higher peak level (up to 400 µM, see appendix). The outflow solutions containing significant levels of ferrous iron were all characterized by the presence of black colloids, which indicates that the measured iron was originated from a particulate phase leaking through the filters. The presence of this iron pulse is observed in case of both pH ranges and showed no systematic dependence on any parameter. The observed pattern for the pH was similar for both pH ranges, showing a slight increase over time.

The total amount of mackinawite formed was calculated for each reactor based on the measured concentration of extractable ferrous iron at the end of the flow-through experiment. After adding this solid phase pool to the total amount of ferrous iron released during the reaction, the percentual progress of the reduction reaction was calculated for each reactor by dividing the result by the total amount of iron measured (including extractable ferric iron after the reaction). This indicated that on average 73 % of the initially available lepidocrocite was reduced on a time scale of about 500 minutes in case of pH 7.5, while this was only about 42 % for a pH of 8.5. The final reaction progress was on average not really different in case of experiments with and without adsorbed phosphate, but varied considerably between parallel reactors. This heterogeneity does not hinder the investigation of the relationship between phosphate release and the reductive dissolution process, but rather enables to consider this relationship in a broader range.

The total amount of ferrous iron produced was also compared to the total amount of elemental sulfur measured in the outflow solutions. Although the resulting molar S^0/Fe(II) ratio was on average larger in case of pH 8.5 than for a pH of 7.5, it was in most cases still much smaller than the expected stoichiometric factor of 0.5 (for more details, see the theoretical section). The potential formation of other further oxidized sulfur species might provide an explanation for the calculated molar S^0/Fe(II) ratios being much smaller than 0.5. In case of reactor 5.6 (pH≈7.5), the concentration of sulfate and thiosulfate species was measured in the outflow solutions as well (Fig. 5.3). Thiosulfate was not observed in case of this experiment. The formation of sulfate seemed to be significant, but the total amount of sulfate observed could not explain the total amount of ferric iron that was reduced in case of this experiment. Elemental sulfur was therefore still recognized as being the dominant reaction

product, but it was likely present as a particulate phase in the reactors. A significant part of the formed reaction product was therefore not measured in the filtrated outflow solutions, which could also explain the molar S^0/Fe(II) to be much smaller than 0.5.

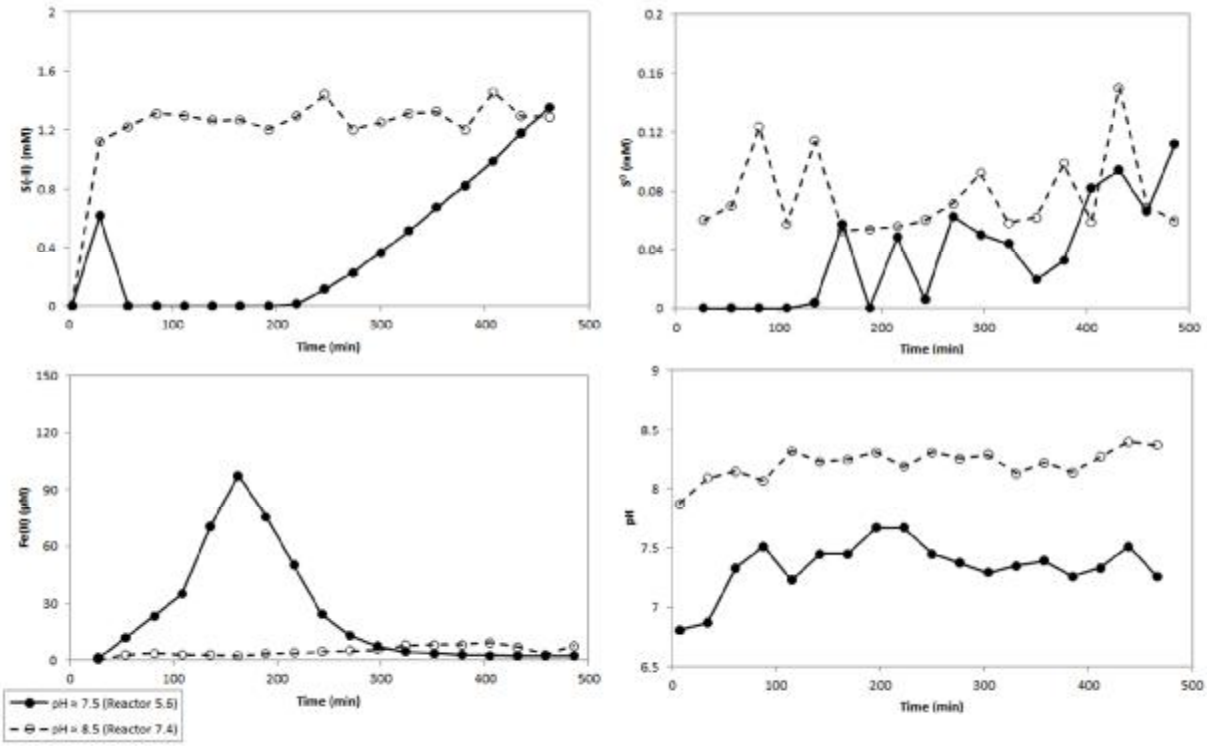

Fig. 5.2. Graphs showing the concentrations of dissolved sulfide, elemental sulfur and ferrous iron measured in the outflow solutions over time, as well as the pH. The two plotted curves show representative data for the two different pH ranges in which the flow-through experiments were performed.

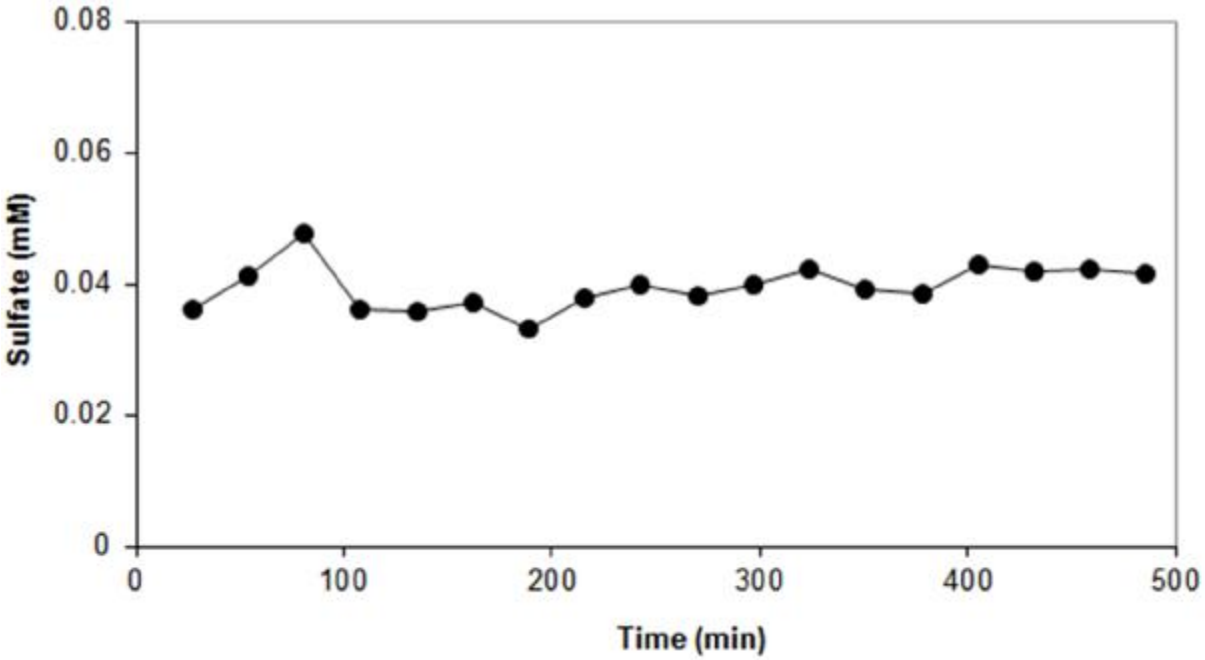

Fig. 5.3. Graph showing the concentration of dissolved sulfate over time in case of reactor 5.6 (pH≈7.5).

5.3. The release of phosphate

In order to consider the release of phosphate separately for the different pools available (bulk and adsorbed phosphate), the breakthrough curves of phosphate were compared for the reactors containing different types of lepidocrocite suspensions. In case of using the lepidocrocite suspension that only contained the bulk type of phosphate, the maximum observed phosphate concentration in the outflow solutions was about 4 µM (Fig. 5.4). The trend observed for the concentration over time was characterized by a relatively fast increase at the beginning, which was mostly followed by a slight decrease towards an almost constant level. Although the difference in the observed values was quite large for the different flow-through experiments performed, all the measured breakthrough curves show concentrations being in the micromolar range that was expected based on the kinetic modeling simulations (Fig. 3.5).

In case of using a lepidocrocite suspension that also contained adsorbed phosphate, the resulting pattern of phosphate release was totally different for the two different pH ranges in which the flow-through experiments were performed (Fig. 5.5). For the reactions taking place at a pH of about 8.5, the release of phosphate was characterized by a peak concentration (up to 12 µM) being observed at the beginning of the flow-through experiment. This observed peak concentration was then followed by a rapid decrease towards much lower values, which were quite constant over time. In case of the reaction taking place at a pH of about 7.5, the initial increase in phosphate concentration was more gradual, with a maximum level of about 7 µM. After the maximum value was reached for a certain experiment, the phosphate concentration was observed to decrease over time towards a final value of about 2 µM (after a time period of about 500 minutes). This decrease was much more gradual than the decrease in phosphate concentration being observed during the reactions taking place at a pH of about 8.5.

Although the observed pattern of phosphate release was completely different for the two pH ranges, the total amount of adsorbed phosphate released during a single flow-through experiment was comparable for both cases. In case of using the lepidocrocite suspension that only contained adsorbed phosphate, on average 73 % of the initial amount of phosphate was released within a time period of about 500 minutes (72 % for a pH of 7.5 and 74 % for a pH of 8.5). Although the amount of phosphate released was a significant portion of the initially adsorbed phosphate pool in case of the flow-through experiments, the observed percentual release was significantly smaller than being expected based on the equilibrium surface speciation of lepidocrocite that was calculated by the model (Fig. 3.2). This indicates that the release of adsorbed phosphate observed for the experiments was at least partially limited by kinetics for both pH ranges.

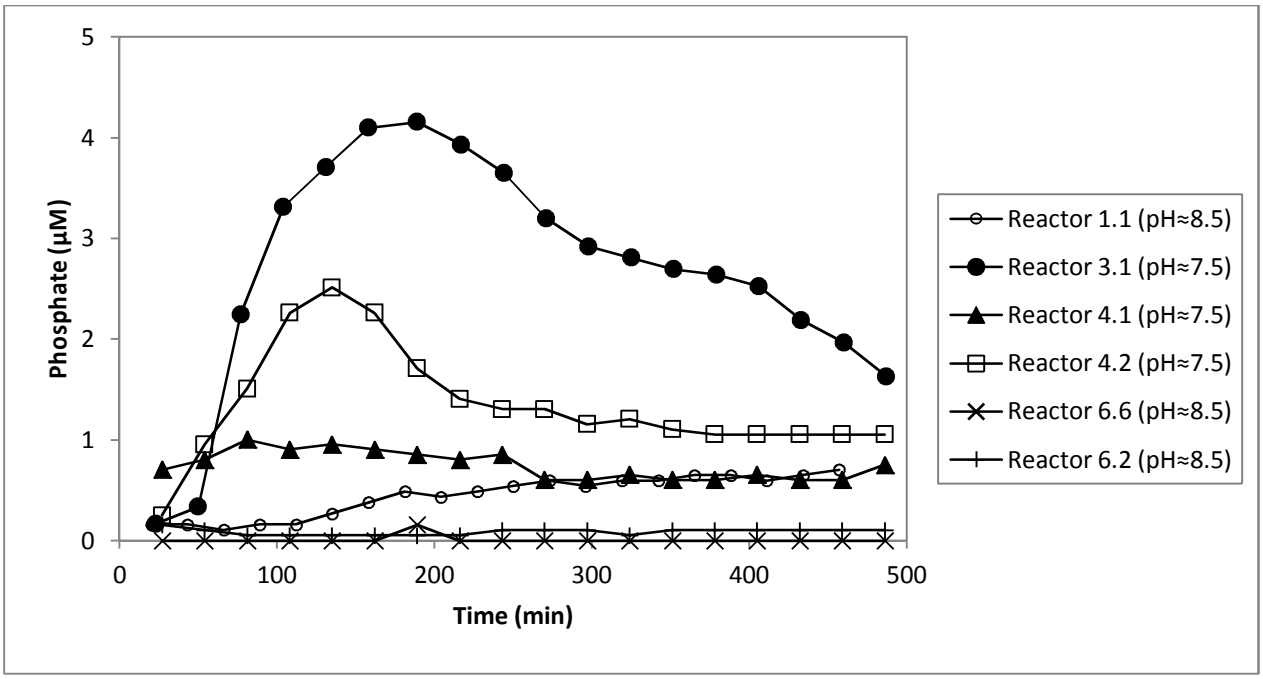

Fig. 5.4. Graph showing the concentration of phosphate over time in the outflow solution, in case of using the lepidocrocite suspension that only contained the bulk type of phosphate.

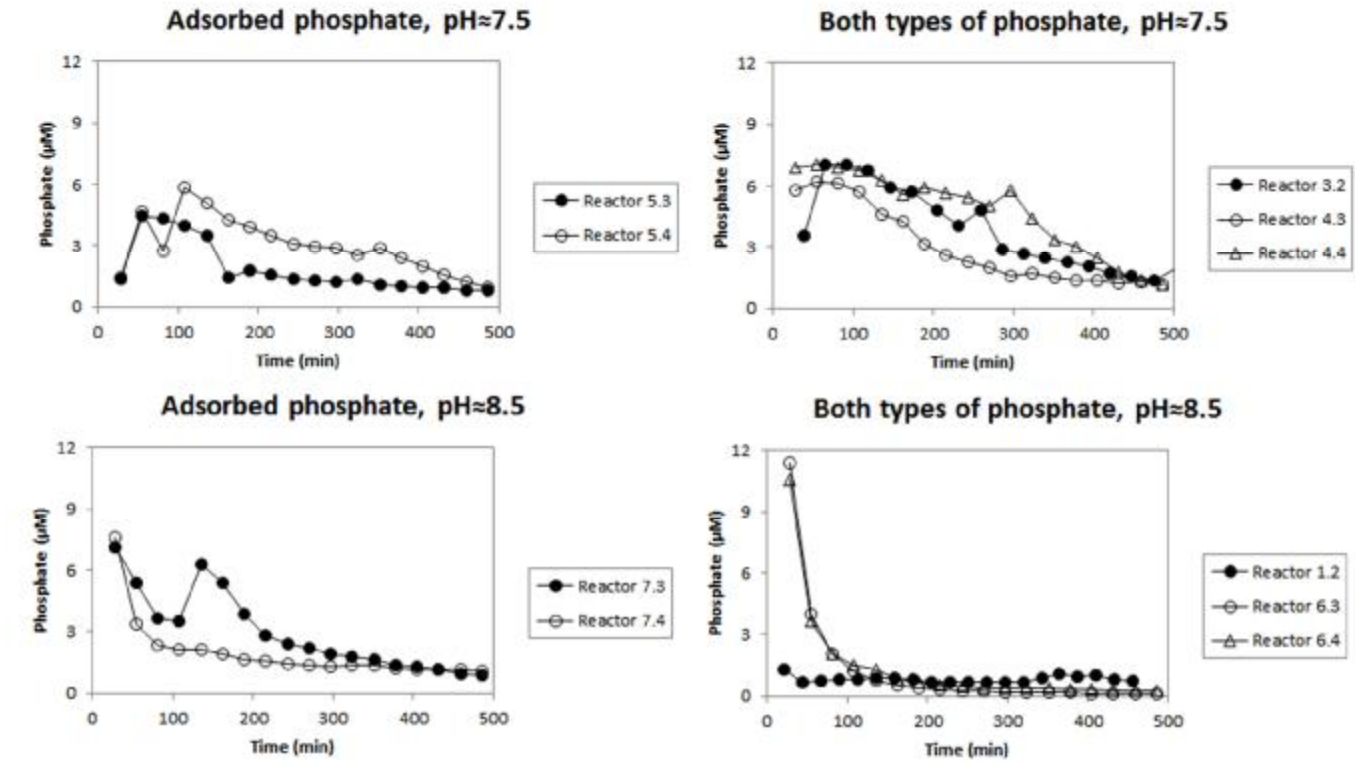

Fig. 5.5. Graphs showing the phosphate concentration over time in the outflow solution, in case of using a lepidocrocite suspension containing either only adsorbed phosphate or both types of phosphate (also including bulk). The results are shown separately for the two different pH ranges in which the concerning flow-through experiments were performed.

5.4. Flow-through experiments with phosphate solution

The results shown in this section are again considered to be representative for all the flow-through experiments with phosphate solution performed (Table 4.2). All the results from this type of flow-through experiments are included in the appendix at the end of this report as well. The effect of phosphate adsorption onto the original lepidocrocite surface is visualized quite well by the resulting breakthrough curves (Fig. 5.6). The breakthrough of phosphate was simply retarded by about 20 minutes for a reactor containing lepidocrocite suspension, when compared to the reactor without lepidocrocite. The retardation was also observed for the reactors containing lepidocrocite type 1, but the effect was then much less pronounced (see appendix).

The situation after the reduction reaction was completely different for the two pH ranges in which the reaction had taken place prior to the flow-through experiments. In case of the reaction taking place at a pH of about 8.5, the resulting breakthrough of phosphate was similar to the breakthrough that was observed for the reactors without lepidocrocite. The total amount of extractable phosphate measured after the second flow-through experiment was comparable to the final amount of aqueous phosphate in this case (calculated from the final concentration). This indicates that no phosphate from the inflow solution was taken up by the mackinawite suspension in the reactor. The situation after the reaction at a pH of about 7.5 was characterized by an almost zero level of phosphate being observed in the outflow solutions after a time period of about 20 minutes. The initial part of the breakthrough curve was similar to the curves measured for the reactors without lepidocrocite in this case, but the maximum concentration reached was only about 1.5 µM. The amount of extractable phosphate measured after the experiment was in this case significant when compared to the total amount of phosphate introduced, which indicates that phosphate was efficiently retained within the reactor.

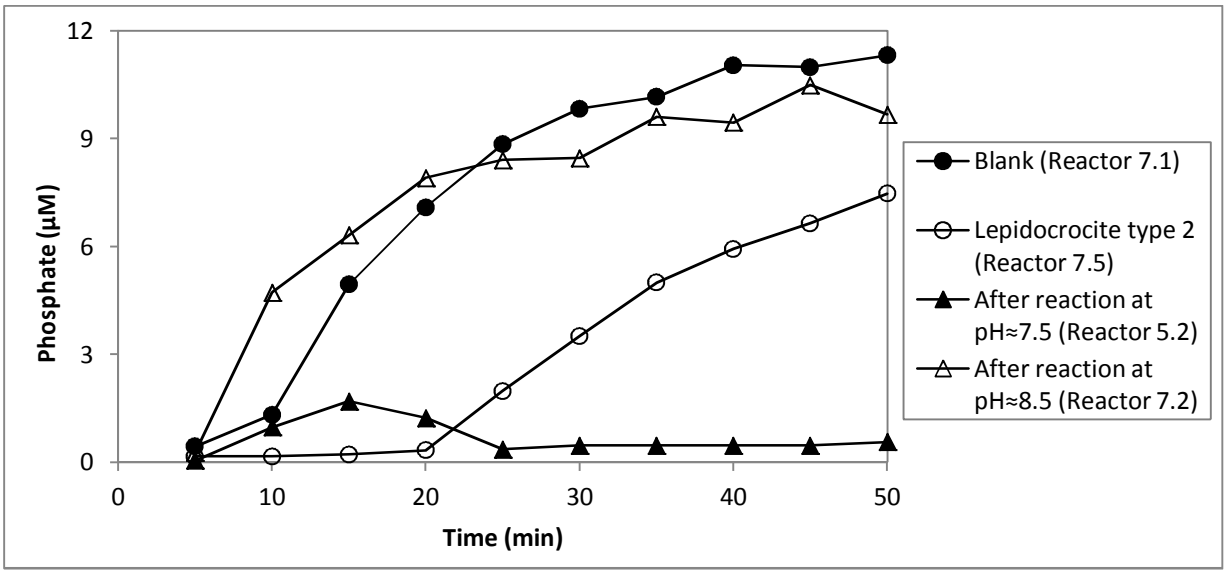

Fig. 5.6. Graph showing the concentration of phosphate over time, as measured for the flow-through experiments with phosphate solution. The data presented here are representative for all the experiments performed.

6. Discussion

6.1. Bulk phosphate release

Based on the mechanism that was proposed for the release of bulk phosphate in the theoretical section, the kinetics of this process are expected to be linearly proportional to the overall rate of the reduction reaction. The total amount of bulk phosphate released during a certain experiment should in this case also be linearly related to the total amount of ferrous iron formed. The total amount of bulk phosphate released was expressed as a fraction of the initial pool for each experiment and the resulting values were plotted against the corresponding final reaction progress, which was calculated as the fraction of iron being reduced at the end of the experiment (Fig. 6.1).

Drawing a straightforward conclusion from this analysis is not allowed because of the relatively small amount of data being included, but the observed linearity in the resulting plot is in accordance to the existence of a linear correlation between the kinetics of bulk phosphate release and the overall reaction rate in case of the flow-through experiments. Based on the assumption of such a linear relationship, the slope that is observed for the linear trend in this plot is expected to be 1. However, the actual slope is significantly smaller (about 0.76), which could not be explained based on the mechanism that was proposed for the release of bulk phosphate.

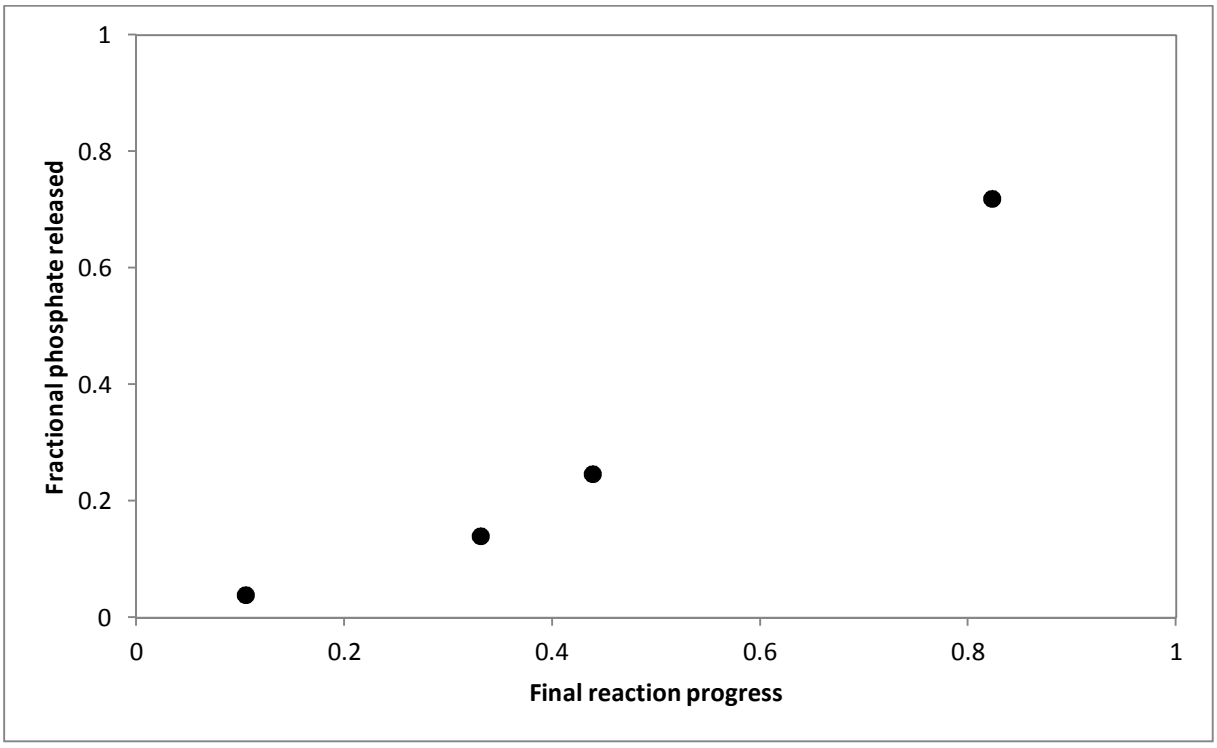

Fig. 6.1. The total amount of phosphate released (normalized to the initial pool available) plotted against the corresponding final reaction progress, in case of using a lepidocrocite suspension that only contained the bulk type of phosphate.

In order to investigate the relationship between the kinetics of the reduction and the process of bulk phosphate release in a more quantitative way, the rates of these two different processes during the flow-through experiments are deduced form the measured breakthrough curves. The influence of anomalous results on the rate calculations is minimized for this analysis by using the moving average over a period of three time steps for the concerning concentration values. For calculating the rate of bulk phosphate release, aqueous phosphate is assumed to be only influenced by this release (to be

calculated) and by the flow out of the concerning reactor, which results in the following differential equation: $dC/dt = v_{release} - QC/V$. The flow rate Q/V is estimated for each time step based on the volume of outflow solution that was collected, as well as based on the volume of the concerning reactor itself. The values for the derivative in the equation above are derived from the concerning breakthrough curves by using the discrete differences between the different measuring points.

The overall rate of the reduction reaction is assumed to be linearly related to the rate of sulfide consumption, which is based on the observations that mackinawite was continuously precipitating during the different flow-through experiments. The rate of sulfide consumption is then estimated for each time step by using the following differential equation: $dC/dt = Q/V \cdot (C_{inflow} - C) - v_{consumption}$. The sulfide concentration in the inflow solution (C_{inflow}) is known for each experiment, while the values for the flow rate and the derivative term are derived from the concerning breakthrough curves. The rate of sulfide consumption is then calculated for each time step by taking the difference between the values for the flow related term and the derivative term. When plotting the values calculated for the rates as a function of time, this results in a good similarity between the patterns that are observed for the two different processes (Fig. 6.2). The calculated rates of phosphate release are all within the range of 0.001 to 0.1 µM/min, while the maximum value reported for the sulfide consumption rate is almost 0.04 mM/min.

Although the large similarity between the two plots described above already implies the presence of a linear relationship between the kinetics of the two concerning processes, this relationship is best visualized by plotting all the calculated rates of phosphate release against the corresponding sulfide consumption rates (Fig. 6.3). The correlation between the rates of the two different processes is even better when only considering the results from the experiments that were performed at a pH of about 7.5. However, the results obtained in case of the reaction taking place at pH≈8.5 do not deviate that much from the trend being observed for the results at pH≈7.5. It is therefore not really clear whether a distinction between the two different pH ranges should be made for describing the process of bulk phosphate release.

This quantitative analysis performed results in the identification of a linear relationship between the kinetics of bulk phosphate release and the overall reduction rate of synthetic lepidocrocite, which is in accordance to the mechanisms proposed in the section on theoretical background. In case of being initially abundant in the bulk phase, phosphate would only be released into solution when it encounters the solid-water interface due to the reductive dissolution of the iron(III) oxyhydroxide phase itself. The total amount of phosphate released is therefore linearly proportional to the final reaction progress of the reductive dissolution reaction, since this could be expressed as the percentual fraction of ferric iron being reduced during the total reaction time.

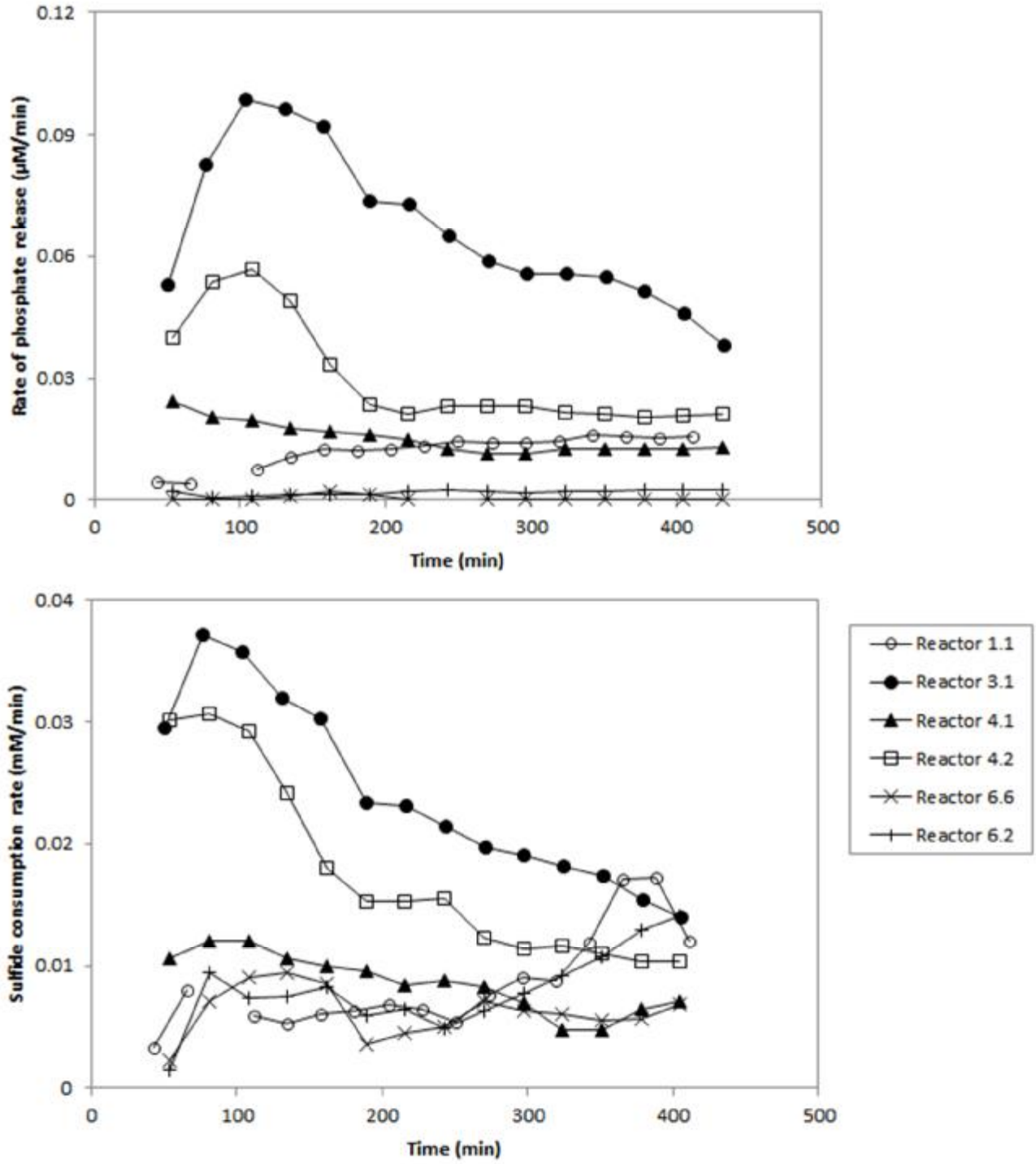

Fig.6.2. Graphs showing the calculated rates of phosphate release (upper plot) and sulfide consumption (lower plot) over time, for the different flow-through experiments with bulk phosphate that were performed.

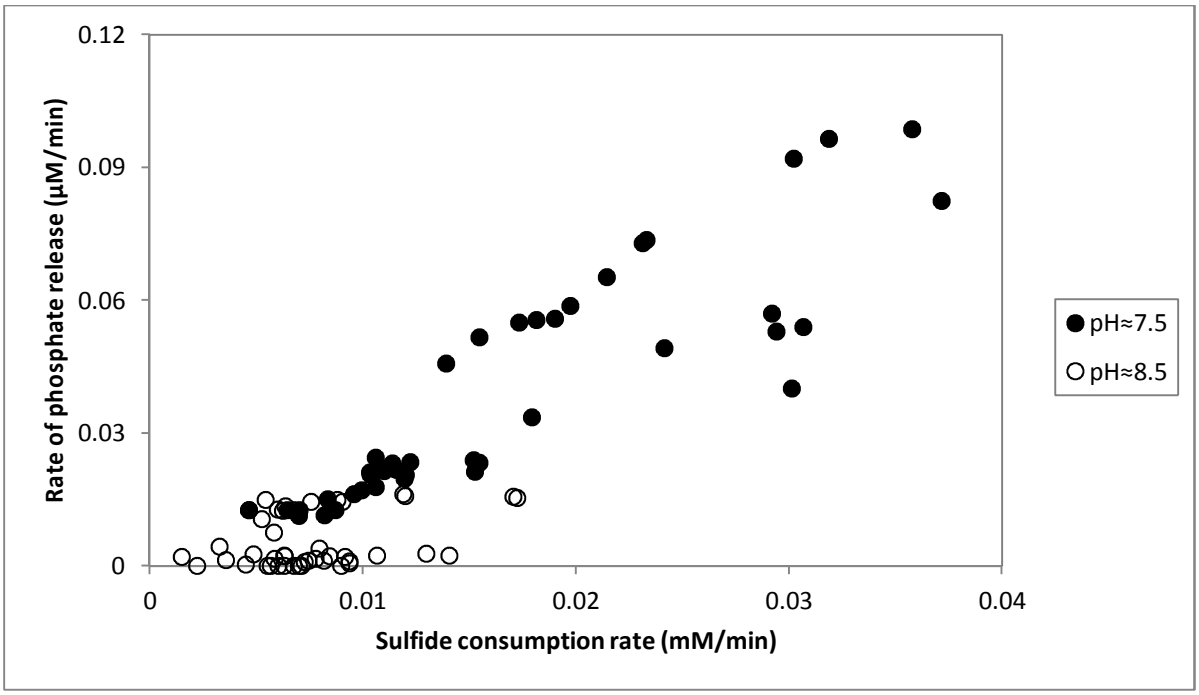

Fig. 6.3. The calculated rates of phosphate release plotted against the corresponding rates of sulfide consumption. The included results are originated from all the performed flow-through experiments with lepidocrocite that only contained bulk phosphate.

6.2. The adsorbed phosphate pool

When considering the final mole balances of phosphate and iron for all the performed flow-through experiments, a significant difference could be observed between the results in case of using different lepidocrocite suspensions (Fig. 6.4). The observed linear relationship between the final reaction progress and the percentual release of bulk phosphate is already discussed in the previous section. Such a linear relationship does not seem to hold in case of using a lepidocrocite suspension that only contained adsorbed phosphate or that contained both types of phosphate. When the progress of the reduction reaction itself is relatively close to 100 percent, phosphate is almost completely released in those cases, which could imply the existence of a correlation between the kinetics of these different processes. However, a superproportional release of phosphate is often observed in case of a low final reaction progress (Fig. 6.4).

The observed pattern of phosphate release at a pH of about 8.5 is quite similar to the results from the modeling simulation in which an instantaneous release of phosphate was considered (compare fig. 3.4 to fig. 5.5). The similarity between the shape of the breakthrough curves that are shown in both plots indicates that the release of adsorbed phosphate should be described as an equilibrium process at a pH of 8.5. Despite the observed similarity in the shape of those curves, the actual levels of phosphate shown are much smaller in case of the flow-through experiments than for the modeling simulation (describing the release of the whole pool). This difference is in accordance to the final mole balances of phosphate for the flow-through experiments, which state that the initial phosphate pool was often not completely released on a time scale of 500 minutes (see appendix). This suggests the existence of two different pools of adsorbed phosphate on the lepidocrocite surface. The release of the so-called labile pool then takes place instantaneously and could be described as an equilibrium process, while the release of the more stable type of pool requires a kinetic description. In case of the performed flow-through experiments, the time scale of release for the more stable type of pool was observed to be longer than 500 minutes at a pH of about 8.5.

Although the initial fast release of adsorbed phosphate from a labile pool is not visualized by the concerning breakthrough curves in case of pH 7.5 (Fig. 5.5), two different pools can be distinguished based on the prevailing rates of phosphate release in this case (Fig. 6.5). The calculation of the rates shown in this plot is done in a similar way as for the analysis on the release of bulk phosphate (see previous section). The rate of adsorbed phosphate release is observed to be much higher during the first 150 minutes than for the remaining parts of the experiments. The rates observed during the initial part of the experiments are also relatively high when compared to the observed rates of bulk phosphate release (Fig. 6.2). The large difference in the rate of adsorbed phosphate release between both periods stated above is in accordance to the existence of a labile and a more stable adsorbed phosphate pool, similar as for the situation at a pH of about 8.5. The anomalous rates of phosphate release during the first 150 minutes then mostly represent the release of the labile pool, while the stable pool is also released during the remaining part of the experiment. The release of these two conceptual pools of adsorbed phosphate is studied separately by considering the first four time steps of the experiments as an individual class.

All the rates of adsorbed phosphate release are then plotted against the corresponding rates of sulfide consumption, which are deduced from the concerning breakthrough curves of sulfide (Fig. 6.6). This plot shows a relatively good linear correlation between both rates for the remaining part of the experiments (after the fourth time step), which indicates that the release of the stable adsorbed phosphate pool is controlled by the overall rate of the reduction reaction. This could be explained by the ligand-exchange rate being smaller than the overall reduction rate of lepidocrocite in case of the stable pool. The kinetic description of the competitive adsorption process itself could therefore not be deduced from the experimental results. The much higher rates of phosphate release for the initial parts of the experiments do not show any correlation to the prevailing rates of sulfide consumption. This could be explained by these rates being largely influenced by the release of the labile phosphate pool, as was already discussed.

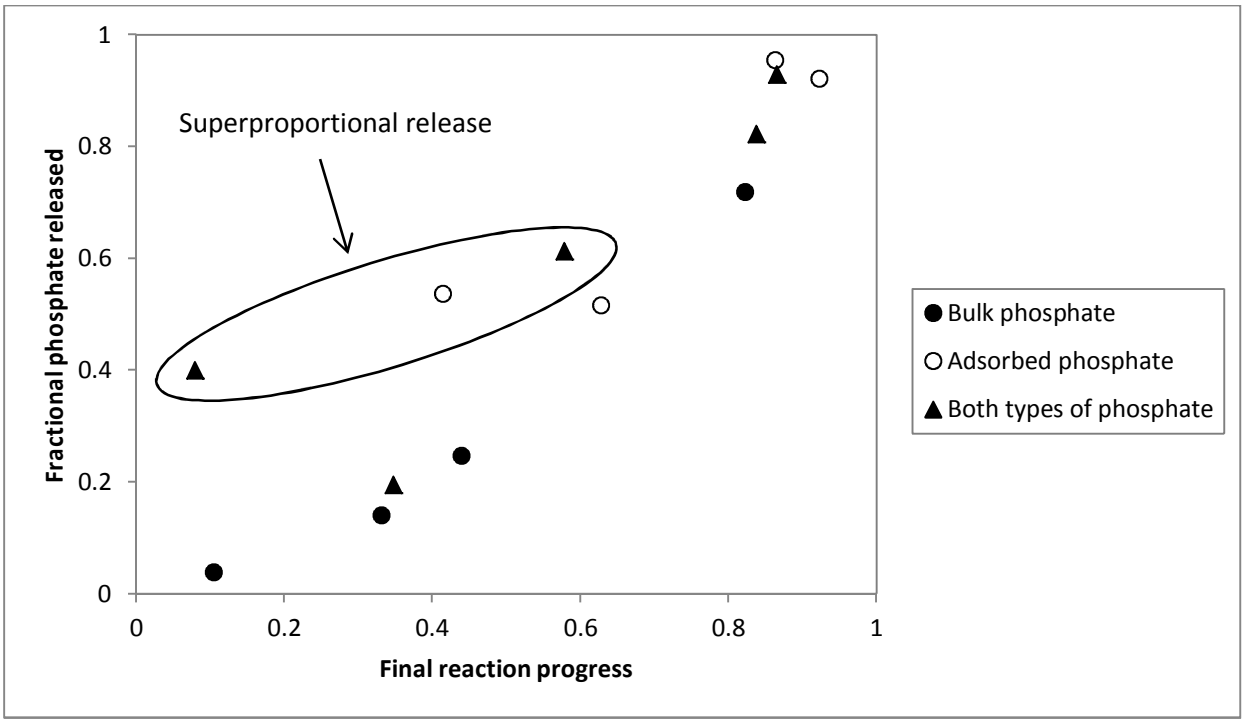

Fig. 6.4. The total amount of phosphate released (normalized to the initial pool available) plotted against the corresponding final reaction progress.

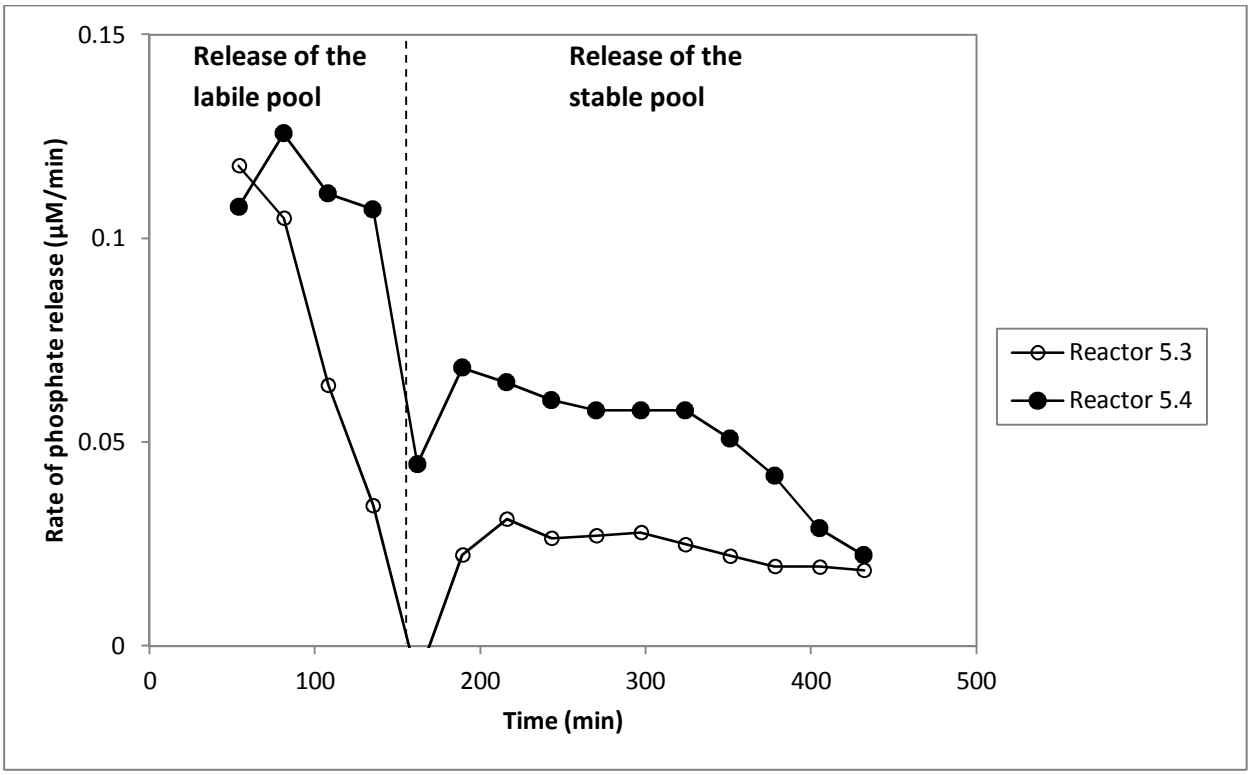

Fig.6.5. Graph showing the calculated rates of phosphate release over time for the two different flow-through experiments with adsorbed phosphate that were performed at a pH of about 7.5.

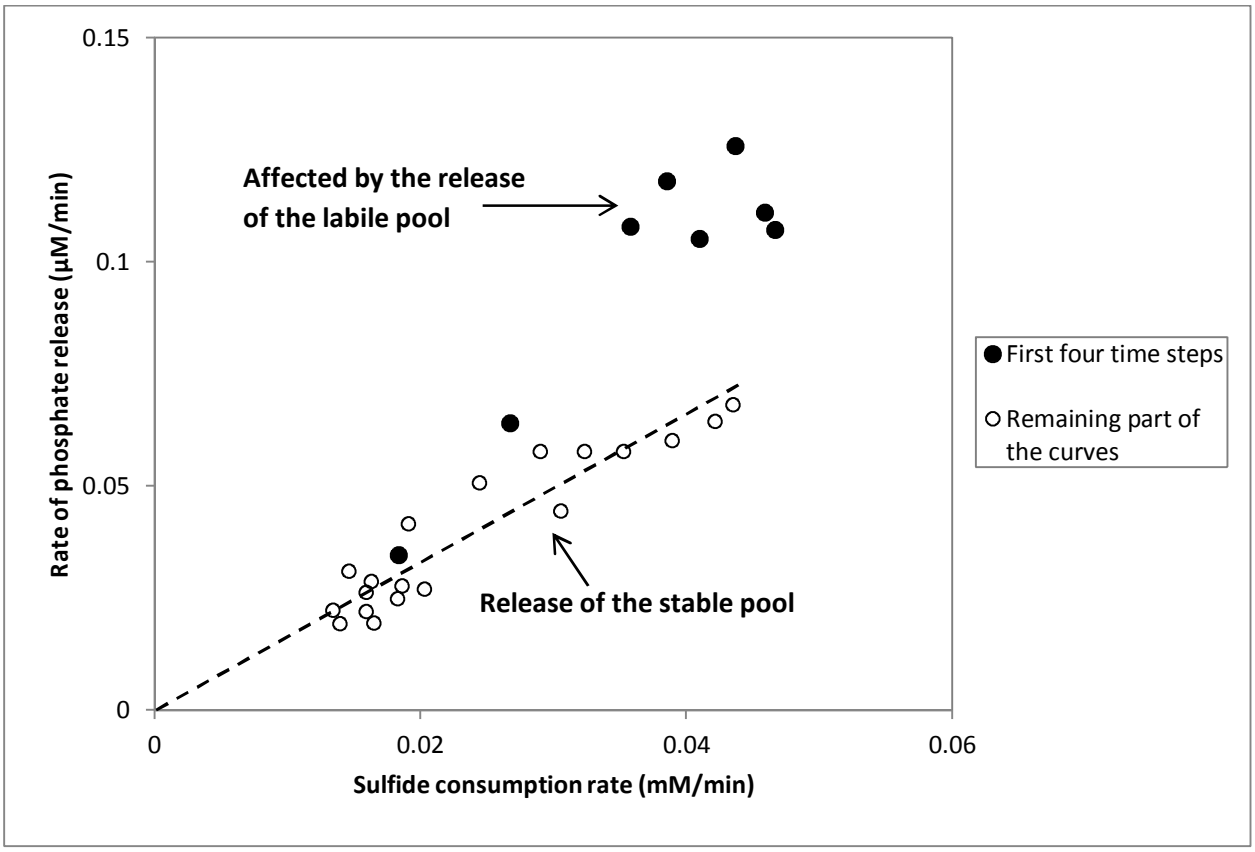

Fig. 6.6. The calculated rates of phosphate release plotted against the corresponding sulfide consumption rates. The results are originated from the two flow-through experiments with lepidocrocite that only contained adsorbed phosphate.

The existence of two different adsorbed phosphate pools in terms of their kinetics of release can be attributed to the coordination of phosphate complexes on the lepidocrocite surface. Based on the background provided in the theoretical section, the release of adsorbed phosphate is expected to take place by two different mechanisms that may occur in parallel: ligand exchange for a bidentate and for a monodentate surface complex. The different patterns observed for the release of adsorbed phosphate could be explained in a relatively simple way by assuming that the previously described labile pool represents the monodentate complexes, while the bidentates are considered to be the stable pool. The concept of these bidentate complexes being less reactive species has been reported earlier, with binuclear surface complexes of oxyanions being considered as an inhibitor for both the reductive and the non-reductive dissolution reaction of various iron(III) oxyhydroxide minerals (Biber et al., 1994). The phosphate release from the bidentate complexes is then completely controlled by the rate of the reaction between lepidocrocite and dissolved sulfide, which is due to the slow kinetics of the competitive adsorption process in this case. The release of phosphate occurs much faster for the monodentate complexes, which leads to the labile pool being totally released during the first 150 minutes of the experiments.

The concept of the monodentate complexes representing the labile phosphate pool also provides an explanation for the large difference in the pattern of adsorbed phosphate release that was observed in case of the two different pH ranges. The phosphate on the lepidocrocite surface is supposed to almost entirely consist of bidentate complexes at a pH of about 7.5, while the relative importance of the monodentate species is expected to become relatively significant in case of pH 8.5 (Fig. 2.3). As discussed in the section on theoretical background, the rate of adsorbed phosphate release from the monodentate complex due to ligand exchange is expected to be described by the following rate law: $v_{release} = k[>FeOPO_3^{2-}][HS^-]$. The relatively large abundance of monodentate complexes then results in the instantaneous type of pattern (large rate of release) that is observed in case of pH 8.5. The initial rate of adsorbed phosphate release is much smaller at pH 7.5, which is due to the almost negligible importance of the monodentate surface complex in this case.

The abundance of the monodentate complex at the lepidocrocite surface is now easily recognized as the most important parameter for explaining the difference in the rate of phosphate release that is observed for the two different pH ranges. The aqueous concentration of bisulfide ions also depends on pH, but the effect on the rate of phosphate release is expected to be considerably smaller, since the concerning values only differ by a factor 1.25 in case of pH 7.5 and 8.5 (Fig. 6.7). The variations in the size of these two parameters being expected based on theory are completely able to explain the difference observed for the pattern of adsorbed phosphate release in case of the two pH ranges. The release of phosphate from the monodentate surface complexes due to ligand exchange takes place instantaneously at a pH of 8.5, while this process is significantly slower in case of pH 7.5.

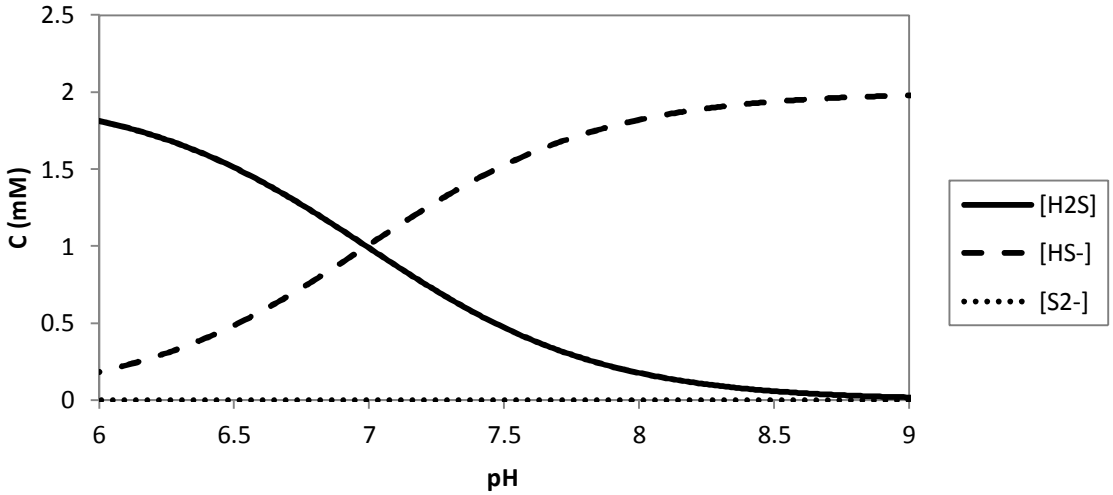

Fig. 6.7. The calculated speciation of a 2 mM dissolved sulfide solution, depending on the prevailing pH. The acid dissociation constants used are pK_1 = 6.99 and pK_2 = 12.92 (Ball and Nordstrom, 1991).

6.3. Retention mechanisms of released phosphate

The potential influence of a certain phosphate retention mechanism on the resulting breakthrough curves of phosphate is not taken into account during the analysis of the results from the first type of flow-through experiments in the previous sections. In order to evaluate whether the influence of any retention mechanism should be considered as being significant in this case, the potential role of the two different proposed retention mechanisms during the reduction reaction is investigated in more detail. This analysis is then based on the results from the various flow-through experiments with phosphate solution that were performed. The importance of phosphate adsorption onto the surface of mackinawite was really excluded by the results from the flow-through experiments performed at a pH of 8, which do not show any retention of the phosphate that was initially introduced. This process is then also expected to be unimportant at a pH of 7, which is confirmed from the initial part of the breakthrough curves in this case (Fig. 5.6). The fraction of the initially introduced phosphate being retained at a pH of 7 should therefore be related to the formation of vivianite, instead of phosphate adsorption onto the formed mackinawite.

The concept of vivianite formation could also explain the almost zero level of phosphate being only observed in the outflow solutions during the second part of the experiment. The lack of vivianite formation in the initial part of the experiments is then simply due to a significant level of dissolved sulfide still being present in the reactors. The sulfide concentration then decreased over time during the flow-through experiment with phosphate solution, which enabled the formation of vivianite out of mackinawite at a certain point. A simple consideration on the thermodynamics of the concerning reaction indicates equilibrium sulfide concentrations of about 8 µM and 4 µM for the experimental conditions at respectively pH 7 and pH 8 (for the constant used, see the theoretical section; Nriagu, 1971). Since the difference between those two values is relatively small, the equilibrium speciation (vivianite or mackinawite being dominant) is expected to be similar for both pH ranges in which the flow-through experiments were performed. The differential behavior that is observed (no vivianite formation at pH 8) could therefore only be explained by a significant influence of the prevailing pH on the kinetics of this process. Despite the observation of vivianite formation at a pH of 7, the results from these experiments indicate that both proposed retention mechanisms are unimportant in case of the reaction between lepidocrocite and dissolved sulfide.

7. Conclusions

Based on the analysis of the modeling study and the experimental results, two different mechanisms of phosphate release have been identified for the reaction between dissolved sulfide and synthetic lepidocrocite. The competitive adsorption process can be described as a ligand exchange reaction in which primarily adsorbed phosphate complexes are replaced by surface complexes of the sulfide that is introduced in the aqueous phase. This process is characterized by relatively fast kinetics in case of a mononuclear surface complex, while the binuclear complexes of phosphate are replaced much more slowly. The kinetics of the second type of mechanism are closely related to the overall reduction rate of the lepidocrocite phase. Phosphate is then only released upon the dissolution of the iron atoms in its close surroundings. Apart from the release of phosphate that is initially situated in the bulk phase, this mechanism also accounts for the release of adsorbed phosphate when the kinetics of the firstly described competitive adsorption process are slower than the dissolution rate of lepidocrocite.

The prevailing pH has a major influence on the observed pattern of phosphate release induced by the introduction of dissolved sulfide. This could be explained by the speciation of phosphate complexes on the lepidocrocite surface, which shows an increasing relative abundance of mononuclear surface complexes when the pH rises above the isoelectric point. Since the competitive adsorption process takes place much faster in case of a mononuclear complex, this results in a more instantaneous type of pattern for the release of adsorbed phosphate in higher pH ranges. The kinetics of ligand exchange in case of a binuclear surface complex are even slower than the dissolution rate of the lepidocrocite phase, which results in a linear correlation between the adsorbed phosphate release and the process of sulfide consumption when the pH is below the isoelectric point.

8. References

Ball, J.W. and Nordstrom, D.K., 1991. User's manual for WATEQ4F, with revised thermodynamic data base and test cases for calculating speciation of major, trace, and redox elements in natural waters. U.S. Geological Survey Open-File Report 91-183.

Biber, M.V., Dos Santos Afonso, M. and Stumm, W., 1994. The coordination chemistry of weathering: IV. Inhibition of the dissolution of oxide minerals. Geochimica et Cosmochimica Acta 58(9): 1999-2010.

Canfield, D.E., 1989. Reactive iron in marine sediments. Geochimica et Cosmochimica Acta 53(3): 619-632.

Chitrakar, R., Tezuka, S., Sonoda, A., Sakane, K., Ooi, K. and Hirotsu, T., 2006. Phosphate adsorption on synthetic goethite and akaganeite. Journal of Colloid and Interface Science 298(2): 602-608.

Cornell, R.M. and Schwertmann, U., 1996. The iron oxides: structure, properties, reactions, occurrence and uses.

Davison, W., Phillips, N. and Tabner, B.J., 1999. Soluble iron sulfide species in natural waters: reappraisal of their stoichiometry and stability constants. Aquatic Sciences 61(1): 23-43.

Diaz, R.J. and Rosenberg, R., 2008. Spreading dead zones and consequences for marine ecosystems. Science 321(5891): 926-929.

Ding, X., Song, X. and Boily, J.F., 2012. Identification of fluoride and phosphate binding sites at FeOOH surfaces. Journal of Physical Chemistry 116(41): 21939 - 21947.

Dos Santos Afonso, M. and Stumm, W., 1992. Reductive dissolution of iron(III) (hydr)oxides by hydrogen sulfide. Langmuir 8(6): 1671-1675.

Dzombak, D.A. and Morel, F.M.M., 1990. Surface complexation modeling: hydrous ferric oxide.

Eckert, B. and Steudel, R., 2003. Molecular spectra of sulfur molecules and solid sulfur allotropes. Topics in current chemistry 231: 31-98.

Gallegos, T.J., Sung, P.H. and Hayes, K.F., 2007. Spectroscopic investigation of the uptake of arsenite from solution by synthetic mackinawite. Environmental Science and Technology 41(21): 7781-7786.

Gupta, S.K., 1976. Über die Phosphat - Elimination in den Systemen H_3PO_4 – γ – FeO(OH) und die Eigenschaften von Klaerschlamm Phosphat. Ph.D. Thesis, Bern University, Switzerland.

Han, D.S., Batchelor, B. and Abdel-Wahab, A., 2011. Sorption of selenium(IV) and selenium(VI) to mackinawite (FeS): effect of contact time, extent of removal, sorption envelopes. Journal of Hazardous Materials 186(1): 451-457.

Hellige, K., Pollok, K., Larese-Casanova, P., Behrends, T. and Peiffer, S., 2012. Pathways of ferrous iron mineral formation upon sulfidation of lepidocrocite surfaces. Geochimica et Cosmochimica Acta 81: 69-81.

Hiemstra, T., Antelo, J., Rahnemaie, R. and Van Riemsdijk, W.H., 2010. Nanoparticles in natural systems I: the effective reactive surface area of the natural oxide fraction in field samples. Geochimica et Cosmochimica Acta 74(1): 41-58.

Hiemstra, T. and Van Riemsdijk, W.H., 1996. A surface structural approach to ion adsorption: the charge distribution (CD) model. Journal of Colloid and Interface Science 179(2): 488-508.

Hiemstra, T. and Van Riemsdijk, W.H., 1999. Surface structural ion adsorption modeling of competitive binding of oxyanions by metal (hydr)oxides. Journal of Colloid and Interface Science 210(1): 182-193.

Kim, J., Li, W., Philips, B.L. and Grey, C.P., 2011. Phosphate adsorption on the iron oxyhydroxides goethite (α-FeOOH), akaganeite (β-FeOOH), and lepidocrocite (γ-FeOOH): a ^{31}P NMR study. Energy & Environmental Science 4(10): 4298-4305.

Koroleff, E., 1983. Determination of phosphorus. In: Methods of Seawater Analysis. Edited by Grasshoff, K., Ehrhardt, M. and Kremling, K.. Verslag Chemie: 117-122.
Lawrence, N.S., Davis, J. and Compton, R.G., 2000. Analytical strategies for the detection of sulfide: a review. Talanta 52(5): 771-784.
Lewis, D.G. and Farmer, V.C., 1986. Infrared absorption of surface hydroxyl groups and lattice vibrations in lepidocrocite (γ-FeOOH) and Boehmite (γ-AlOOH). Clay Minerals 21(1): 93-100.
Morel, F.M.M. and Hering, J.G., 1993. Principles and applications of aquatic chemistry.
Nriagu, J.O., 1971. Stability of vivianite and ion-pair formation in the system $Fe_3(PO_4)_2 – H_3PO_4 – H_2O$. Geochimica et Cosmochimica Acta 36(4): 459-470.
Parkhurst, D.L. and Appelo, C.A.J., 1999. User's guide to PHREEQC (version 2) – a computer program for speciation, batch-reaction, one-dimensional transport, and inverse geochemical calculations. U.S. Geological Survey Water-Resources Investigations Report 99-4259.
Peiffer, S., Dos Santos Afonso, M., Wehrli, B. and Gächter, R., 1992. Kinetics and mechanism of the reaction of H_2S with lepidocrocite. Environmental Science and Technology 26(12): 2408-2413.
Poulton, S.W., 2003. Sulfide oxidation and iron dissolution kinetics during the reaction of dissolved sulfide with ferrihydrite. Chemical Geology 202(1-2): 79-94.
Poulton, S.W., Krom, M.D. and Raiswell, R., 2004. A revised scheme for the reactivity of iron (oxyhydr)oxide minerals towards dissolved sulfide. Geochimica et Cosmochimica Acta 68(18): 3703-3715.
Rickard, D., 1995. Kinetics of FeS precipitation: Part 1. Competing reaction mechanisms. Geochimica et Cosmochimica Acta 59(21): 4367-4379.
Rickard, D., 2006. The solubility of FeS. Geochimica et Cosmochimica Acta 70(23): 5779-5789.
Rickard, D. and Luther, G.W., 2007. Chemistry of iron sulfides. Chemical Reviews 107(2): 514-562.
Schwertmann, U. and Cornell, R.M., 2000. Iron oxides in the laboratory: preparation and characterization.
Roncal-Herrero, T., Rodríguez-Blanco, J.D., Benning, L.G. and Oelkers, E.H., 1996. Precipitation of iron and aluminum phosphates directly from aqueous solution as a function of temperature from 50 to 200 °C. Crystal Growth and Design 9(12): 5197-5205.
Tanada, S., Kabayama, M., Kawasaki, N., Sakiyama, T., Nakamura, T., Araki, M. and Tamura, T., 2003. Removal of phosphate by aluminum oxide hydroxide. Journal of Colloid and Interface Science 257(1): 135-140.
Tejedor-Tejedor, M.I. and Anderson, M.A., 1990. Protonation of phosphate on the surface of goethite as studied by CIR-FTIR and electrophoretic mobility. Langmuir 6(3): 602-611.
Viollier, E., Inglett, P.W., Hunter, K., Roychoudhury, A.N. and Van Cappellen, P., 2000. The ferrozine method revisited: Fe(II)/Fe(III) determination in natural waters. Applied Geochemistry 15(6): 785-790.
Weng, L., Vega, F.A. and Van Riemsdijk, W.H., 2011. Competitive and synergistic effects in pH dependent phosphate adsorption in soils: LCD modeling. Environmental Science and Technology 45(19): 8420-8428.
Wolthers, M., Charlet, L., Van der Linde, P.R., Rickard, D. and Van der Weijden, C.H., 2005. Surface chemistry of disordered mackinawite (FeS). Geochimica et Cosmochimica Acta 69(14): 3469-3481.
Yao, W. and Millero, F.J., 1996. Oxidation of hydrogen sulfide by hydrous Fe(III) oxides in seawater. Marine Chemistry 52(1): 1-16.

9. Appendix

A complete overview of the experimental results is included below as an appendix of the report. For each individual flow-through experiment with sulfide solution that was performed, the breakthrough curves of dissolved sulfide, elemental sulfur, ferrous iron and phosphate are presented first. In case of measuring the pH and the sulfate concentration in the outflow solutions over time, these results are included as well. The different mole balances are then included for each of the reactors, showing the total amount of ferrous iron and phosphate produced, as well as the total amount of elemental sulfur that was measured in the outflow solutions. In case of performing a flow-through experiment with phosphate solution afterwards, the concerning results are included as breakthrough curves as well.

Experiment no. 1

Date: 24-09-2012
pH_{inflow} = 8.46
$[S(-II)]_{inflow}$ = 1.99 mM
Reactor 1.1: lepidocrocite type 1 prior to adsorption (bulk phosphate)
Reactor 1.2: lepidocrocite type 1 after adsorption (both types of phosphate)

Breakthrough curves:

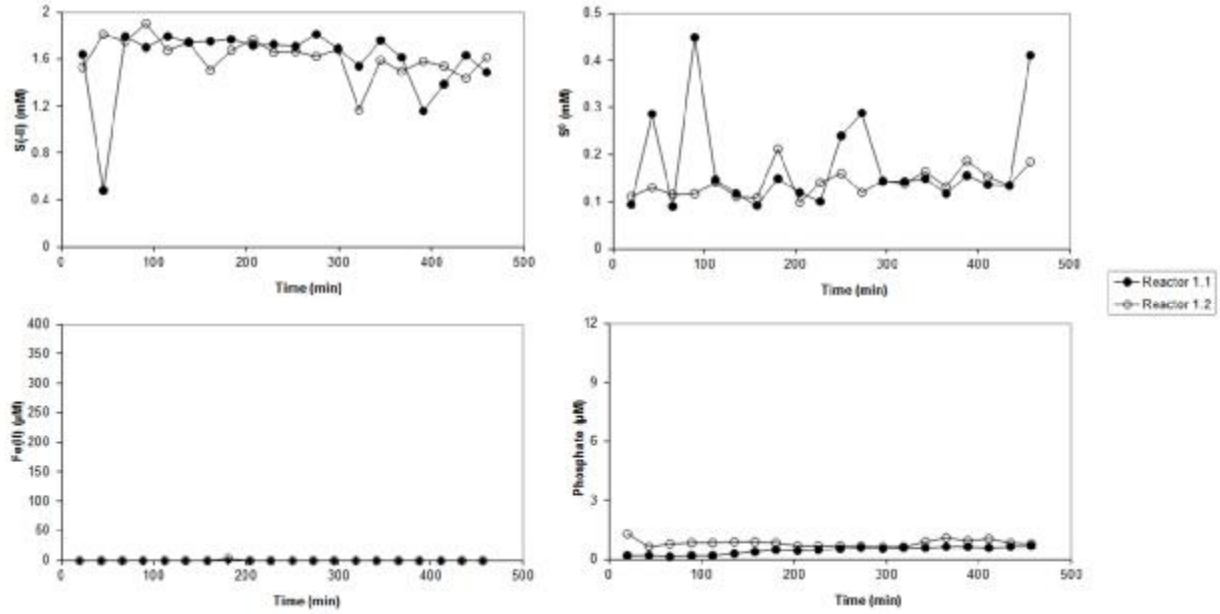

Mole balances:

Reactor 1.1:

Initial Fe(III) = 0.376 mmol
Formed Fe(II) = 0.125 mmol (33 %)

Initial PO_4 = 0.972 µmol
Released PO_4 = 0.136 µmol (14 %)

Total S^0 measured = 0.050 mmol
$S^0_{measured}/Fe(II)_{formed}$ = 0.398

Reactor 1.2:

Initial Fe(III) = 0.379 mmol
Formed Fe(II) = 0.131 mmol (35 %)

Initial PO_4 = 1.301 µmol
Released PO_4 = 0.254 µmol (20 %)

Total S^0 measured = 0.043 mmol
$S^0_{measured}/Fe(II)_{formed}$ = 0.330

Experiment no. 3

Date: 18-10-2012
pH_{inflow} = 7.33
$[S(-II)]_{inflow}$ = 1.95 mM
Reactor 3.1: lepidocrocite type 1 prior to adsorption (bulk phosphate)
Reactor 3.2: lepidocrocite type 1 after adsorption (both types of phosphate)
Reactor 3.3: blank reactor

Breakthrough curves:

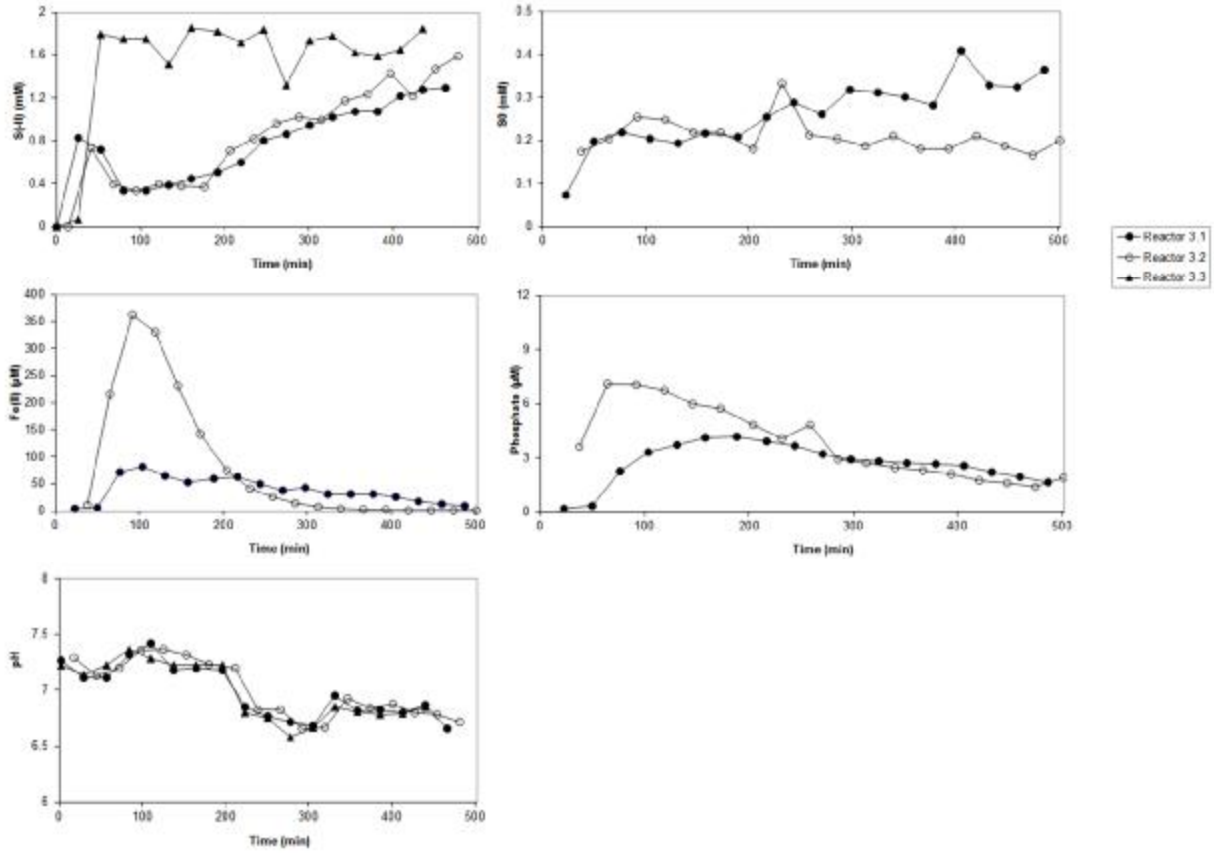

Mole balances:

Reactor 3.1:

Initial Fe(III) = 0.358 mmol
Formed Fe(II) = 0.295 mmol (82 %)

Initial PO_4 = 1.263 µmol
Released PO_4 = 0.907 µmol (72 %)

Total S^0 measured = 0.089 mmol
$S^0_{measured}/Fe(II)_{formed}$ = 0.303

Reactor 3.2:

Initial Fe(III) = 0.319 mmol
Formed Fe(II) = 0.267 mmol (84 %)

Initial PO_4 = 1.810 µmol
Released PO_4 = 1.487 µmol (82 %)

Total S^0 measured = 0.070 mmol
$S^0_{measured}/Fe(II)_{formed}$ = 0.263

Experiment no. 4

Date: 13-11-2012
pH_{inflow} = 7.21
$[S(-II)]_{inflow}$ = 1.92 mM
Reactor 4.1, 4.2 & 4.5: lepidocrocite type 1 prior to adsorption (bulk phosphate)
Reactor 4.3 & 4.4: lepidocrocite type 1 after adsorption (both types of phosphate)
Reactor 4.6: blank reactor

Breakthrough curves:

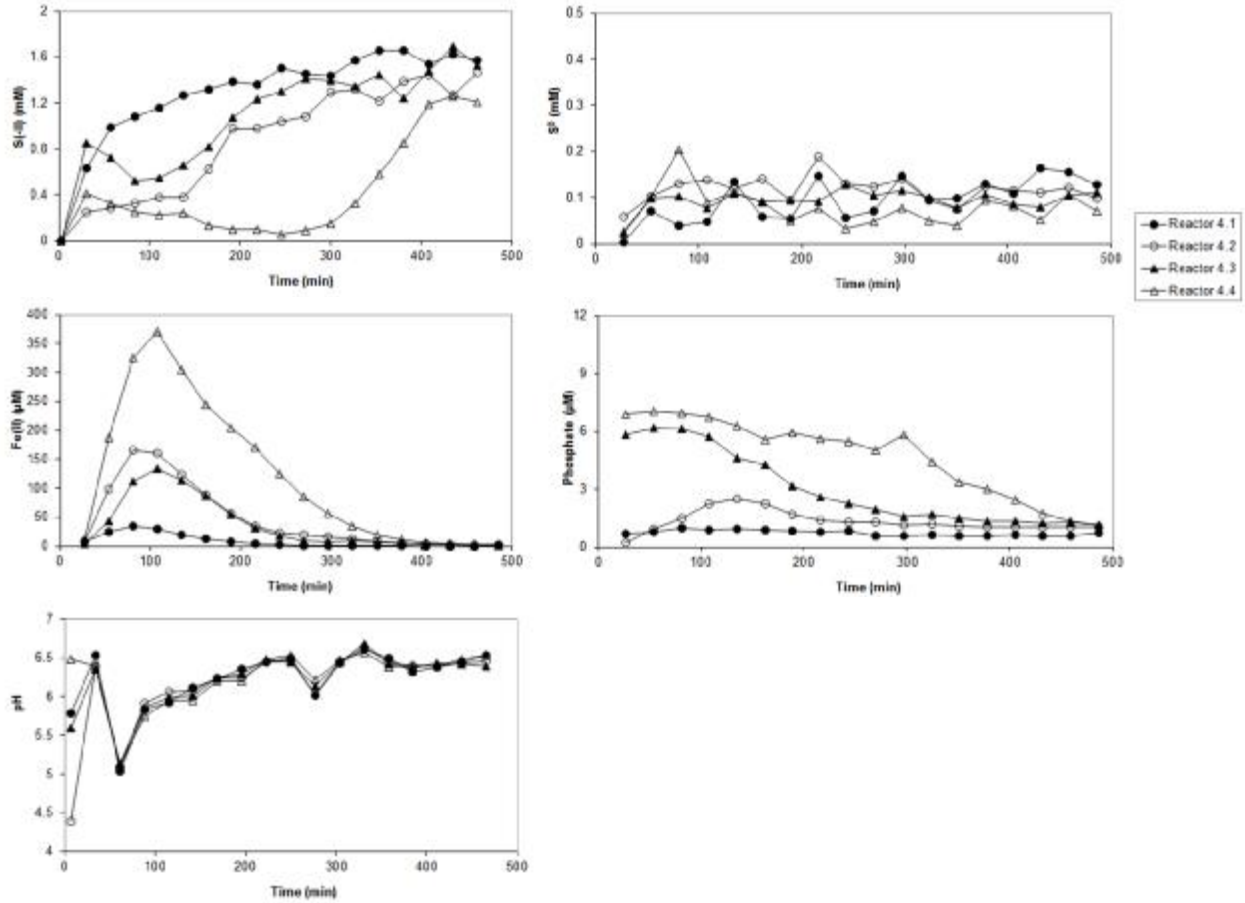

Mole balances:

Reactor 4.1:

Initial Fe(III) = 0.348 mmol
Formed Fe(II) = 0.153 mmol (44 %)

Initial PO_4 = 0.978 µmol
Released PO_4 = 0.240 µmol (25 %)

Total S^0 measured = 0.030 mmol
$S^0_{measured}/Fe(II)_{formed}$ = 0.199

Reactor 4.2:

Initial Fe(III) = 0.326 mmol
Formed Fe(II) = 0.241 mmol (74 %)

PO_4 measured after second experiment
Released PO_4 = 0.454 µmol

Total S^0 measured = 0.037 mmol
$S^0_{measured}/Fe(II)_{formed}$ = 0.153

Reactor 4.3:

Initial Fe(III) = 0.360 mmol
Formed Fe(II) = 0.208 mmol (58 %)

Initial PO_4 = 1.886 µmol
Released PO_4 = 1.155 µmol (61 %)

Total S^0 measured = 0.033 mmol
$S^0_{measured}/Fe(II)_{formed}$ = 0.157

Reactor 4.4:

Initial Fe(III) = 0.371 mmol
Formed Fe(II) = 0.321 mmol (87 %)

Initial PO_4 = 1.970 µmol
Released PO_4 = 1.830 µmol (93 %)

Total S^0 measured = 0.026 mmol
$S^0_{measured}/Fe(II)_{formed}$ = 0.080

Results flow-through experiment with phosphate solution:

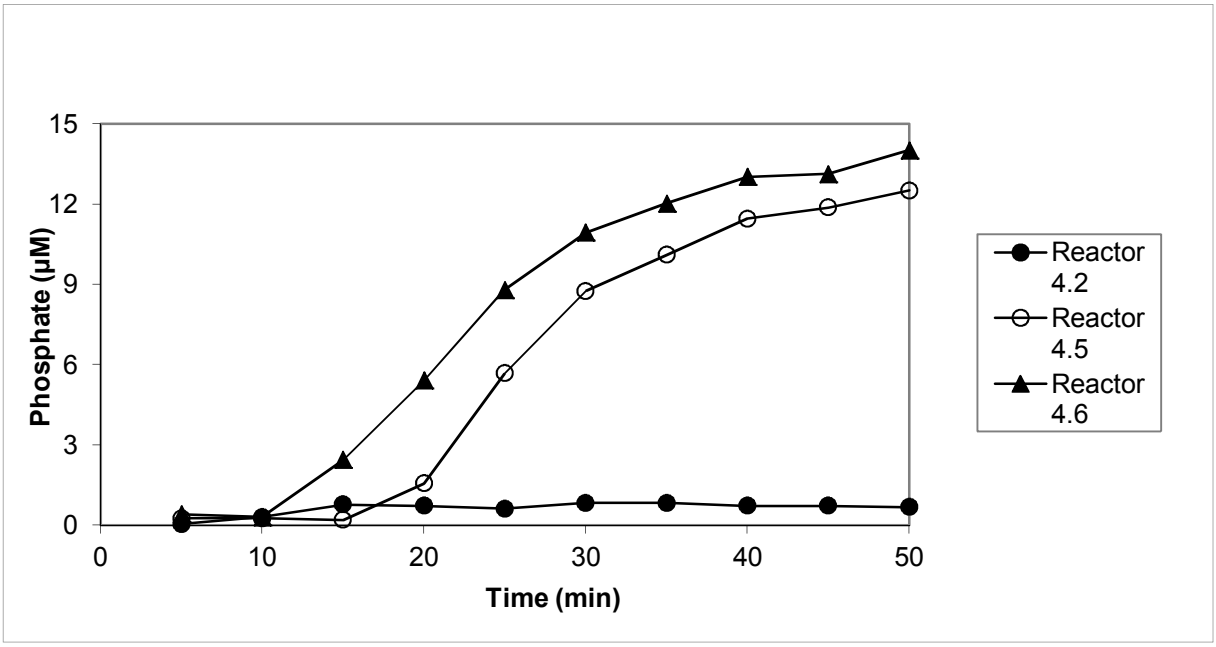

Experiment no. 5

Date: 27-11-2012
pH_{inflow} = 7.09
$[S(-II)]_{inflow}$ = 2.04 mM
Reactor 5.6, 5.2 & 5.5: lepidocrocite type 2 prior to adsorption (no phosphate)
Reactor 5.3 & 5.4: lepidocrocite type 2 after adsorption (adsorbed phosphate)
Reactor 5.1: blank reactor

Breakthrough curves:

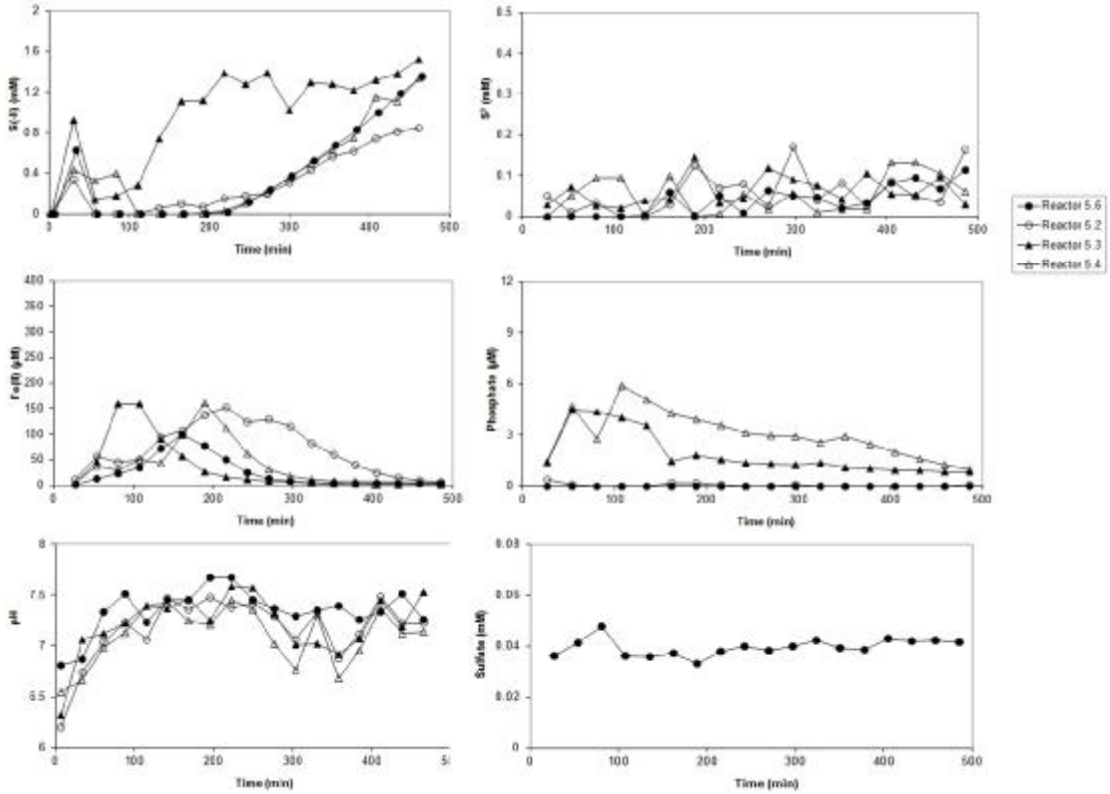

Mole balances:

Reactor 5.6:

Initial Fe(III) = 0.349 mmol
Formed Fe(II) = 0.323 mmol (92 %)

Total S^0 measured = 0.013 mmol
$S^0_{measured}/Fe(II)_{formed}$ = 0.041

Reactor 5.2:

Initial Fe(III) = 0.351 mmol
Formed Fe(II) = 0.327 mmol (93 %)

Total S^0 measured = 0.019 mmol
$S^0_{measured}/Fe(II)_{formed}$ = 0.059

Reactor 5.3:

Initial Fe(III) = 0.300 mmol
Formed Fe(II) = 0.188 mmol (63 %)

Initial PO_4 = 1.278 µmol
Released PO_4 = 0.659 µmol (52 %)

Total S^0 measured = 0.020 mmol
$S^0_{measured}/Fe(II)_{formed}$ = 0.107

Reactor 5.4:

Initial Fe(III) = 0.306 mmol
Formed Fe(II) = 0.283 mmol (92 %)

Initial PO_4 = 1.137 µmol
Released PO_4 = 1.047 µmol (92 %)

Total S^0 measured = 0.017 mmol
$S^0_{measured}/Fe(II)_{formed}$ = 0.061

Results flow-through experiment with phosphate solution:

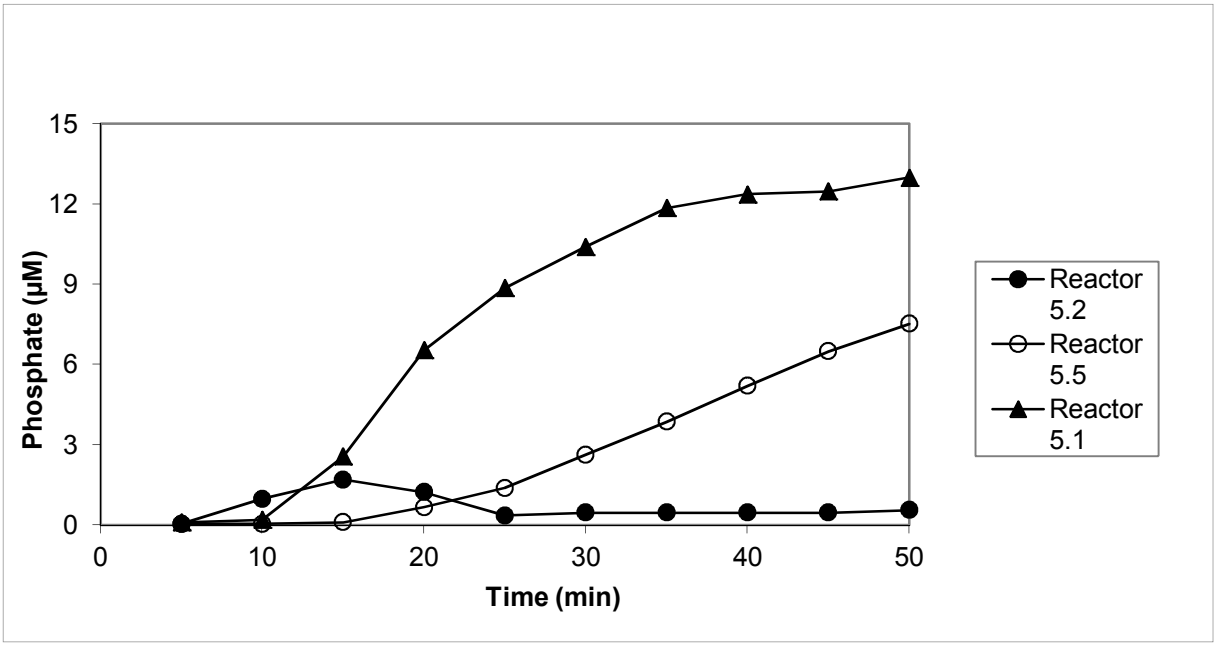

Phosphate introduced: 1.305 µmol
Taken up by reactor 5.2: 0.430 µmol (33 %)
Taken up by reactor 5.5: 0.634 µmol (49 %)

Experiment no. 6

Date: 11-12-2012
pH_{inflow} = 8.31
$[S(-II)]_{inflow}$ = 1.97 mM
Reactor 6.6, 6.2 & 6.5: lepidocrocite type 1 prior to adsorption (bulk phosphate)
Reactor 6.3 & 6.4: lepidocrocite type 1 after adsorption (both types of phosphate)
Reactor 6.1: blank reactor

Breakthrough curves:

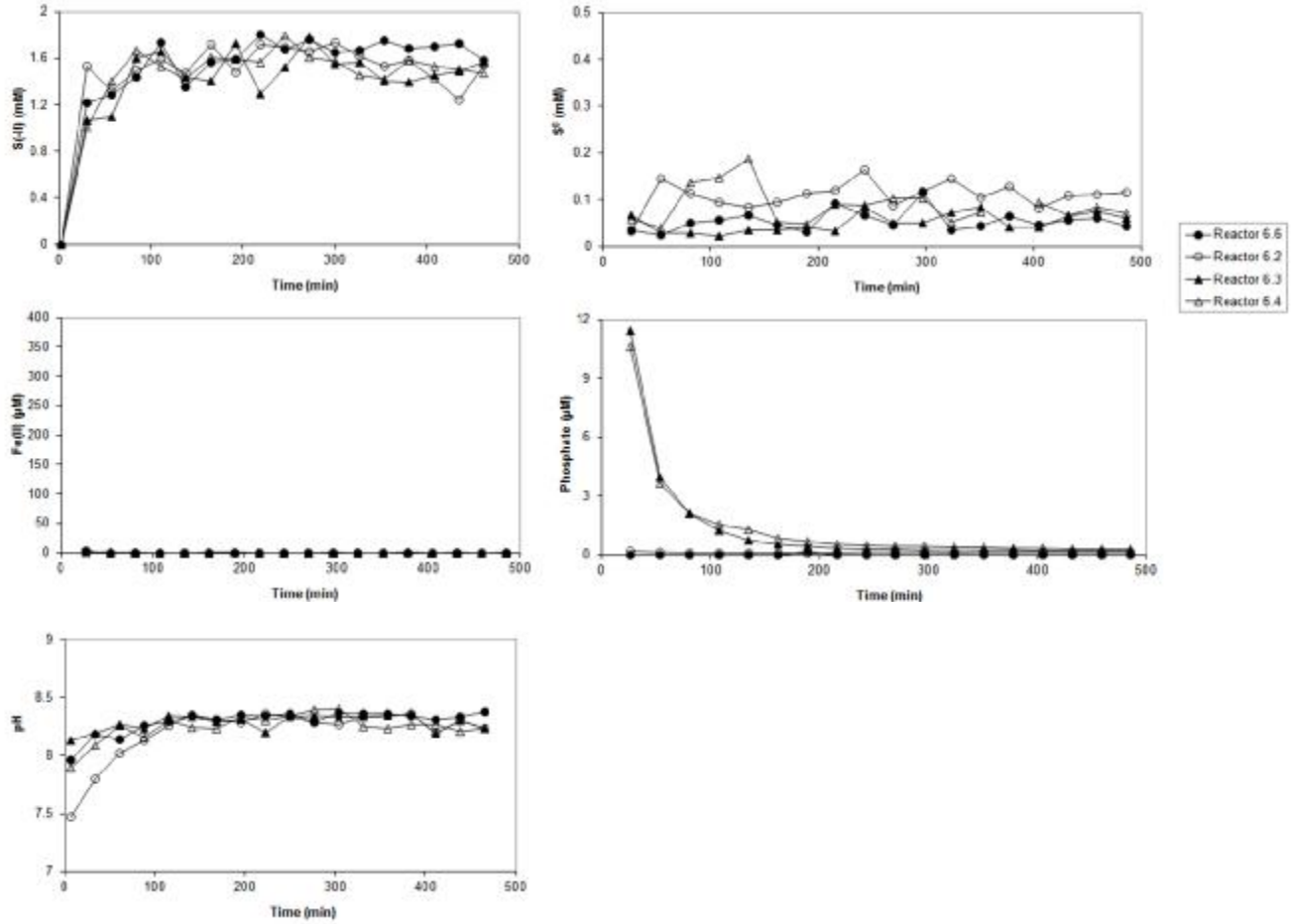

Mole balances:

Reactor 6.2:

Initial Fe(III) = 0.340 mmol
Formed Fe(II) = 0.036 mmol (11 %)

Initial PO_4 = 0.941 µmol
Released PO_4 = 0.036 µmol (4 %)

Total S^0 measured = 0.036 mmol
$S^0_{measured}/Fe(II)_{formed}$ = 0.998

Reactor 6.4:

Initial Fe(III) = 0.323 mmol
Formed Fe(II) = 0.025 mmol (8 %)

Initial PO_4 = 1.868 µmol
Released PO_4 = 0.746 µmol (40 %)

Total S^0 measured = 0.034 mmol
$S^0_{measured}/Fe(II)_{formed}$ = 1.329

Results flow-through experiment with phosphate solution:

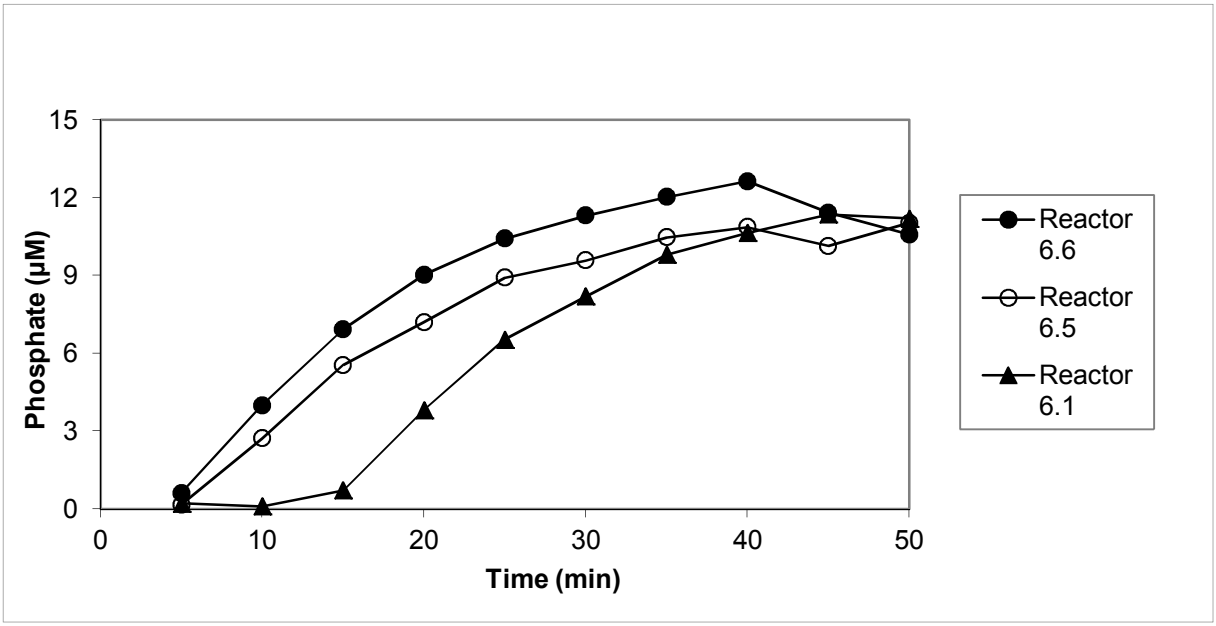

Experiment no. 7

Date: 15-01-2013
pH_{inflow} = 8.39
$[S(-II)]_{inflow}$ = 2.22 mM
Reactor 7.6, 7.2 & 7.5: lepidocrocite type 2 prior to adsorption (no phosphate)
Reactor 7.3 & 7.4: lepidocrocite type 2 after adsorption (adsorbed phosphate)
Reactor 7.1: blank reactor

Breakthrough curves:

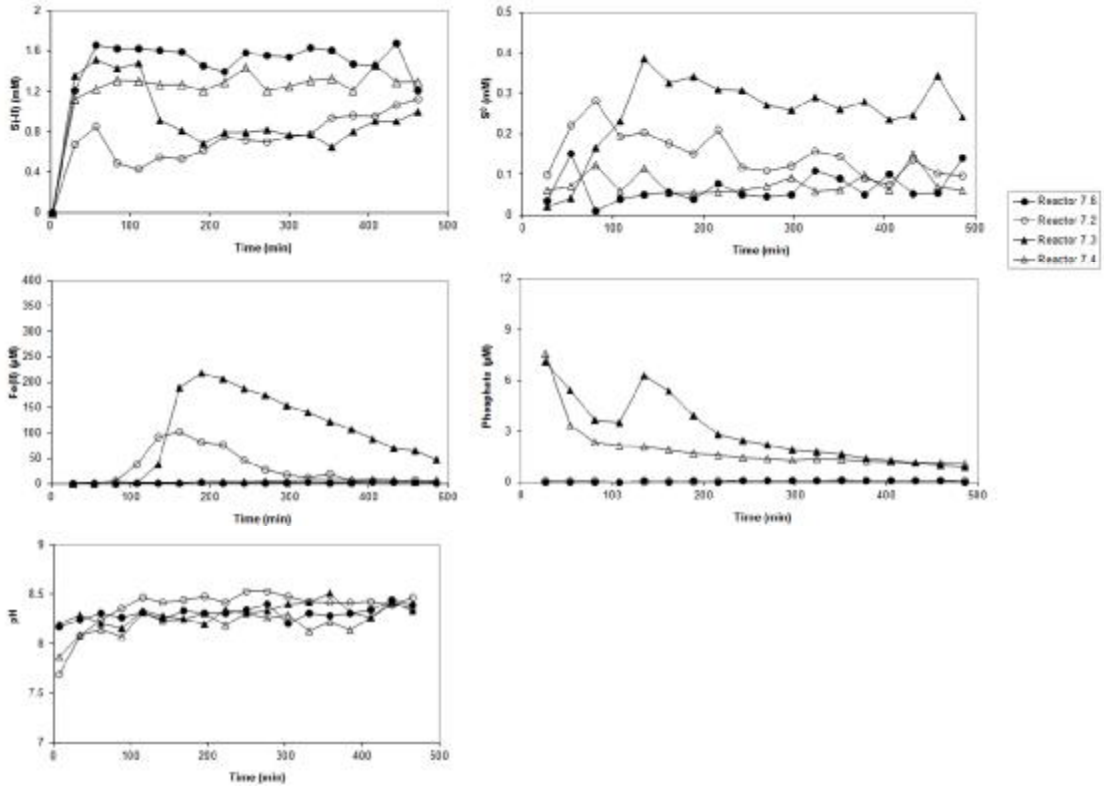

Mole balances:

Reactor 7.6:

Initial Fe(III) = 0.349 mmol
Formed Fe(II) = 0.102 mmol (29 %)

Total S^0 measured = 0.023 mmol
$S^0_{measured}/Fe(II)_{formed}$ = 0.221

Reactor 7.2:

Initial Fe(III) = 0.354 mmol
Formed Fe(II) = 0.298 mmol (84 %)

Total S^0 measured = 0.048 mmol
$S^0_{measured}/Fe(II)_{formed}$ = 0.159

Reactor 7.3:

Initial Fe(III) = 0.306 mmol
Formed Fe(II) = 0.264 mmol (86 %)

Initial PO_4 = 1.225 µmol
Released PO_4 = 1.168 µmol (95 %)

Total S^0 measured = 0.087 mmol
$S^0_{measured}/Fe(II)_{formed}$ = 0.329

Reactor 7.4:

Initial Fe(III) = 0.307 mmol
Formed Fe(II) = 0.127 mmol (41 %)

Initial PO_4 = 1.358 µmol
Released PO_4 = 0.728 µmol (54 %)

Total S^0 measured = 0.025 mmol
$S^0_{measured}/Fe(II)_{formed}$ = 0.194

Results flow-through experiment with phosphate solution:

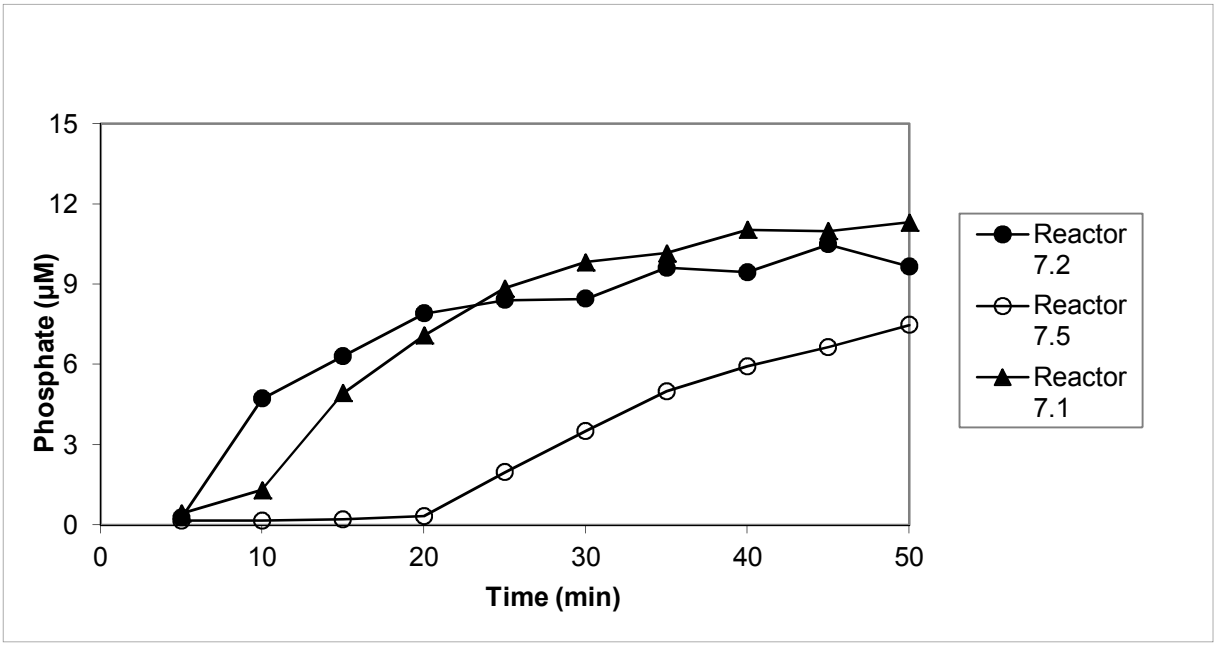

Phosphate introduced: 1.305 µmol
Taken up by reactor 7.2: 0.022 µmol (2 %)
Taken up by reactor 7.5: 0.334 µmol (26 %)